National Defense
Defence nationale

UNCLASSIFIED

DRES

SUFFIELD REPORT

NO. 585

AD-A266 691

UNLIMITED
DISTRIBUTION

ESTIMATION OF DEPTH, ORIENTATION, LENGTH AND DIAMETER OF LONG, HORIZONTAL FERROUS RODS USING A FLUXGATE MAGNETOMETER

by

John E. McFee, Robert Ellingson,
John Elliott and Yogadhish Das

031 SD and 27B77 (Task DMER 15)

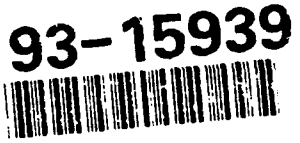

93-15939

April 1993

DEFENCE RESEARCH ESTABLISHMENT SUFFIELD : RALSTON : ALBERTA

Canada

DEFENCE RESEARCH ESTABLISHMENT SUFFIELD
RALSTON, ALBERTA

SUFFIELD REPORT NO. 585

ESTIMATION OF DEPTH, ORIENTATION, LENGTH AND DIAMETER OF LONG, HORIZONTAL FERROUS RODS USING A FLUXGATE MAGNETOMETER

by

John E. McFee, Robert Ellingson, John Elliott and Yogadhish Das

ABSTRACT

A patented hand-held instrument has been built that is the first instrument to explicitly locate ferrous rods parallel to and buried behind or beneath a plane of measurement by analysing magnetic field and position data. The instrument has several useful applications, in particular the detection and characterization of reinforcing steel in concrete.

The instrument consists of a fluxgate magnetometer and position sensor unit enclosed in a small box which is moved by hand somewhat like a computer mouse. A cable connects the sensor unit to a processor unit, containing a microprocessor, A/D, displays and batteries. An operator scans the sensor unit over the measurement surface, guided by the microprocessor, which controls the simultaneous collection of magnetic and position data. The microprocessor then uses simple algorithms to estimate location parameters, rod length and diameter.

This report describes the final version of the instrument. Experimental magnetic data from horizontal rods are presented and compared to two simple models, the infinite cylinder and the long prolate spheroid. It was found that there was very poor agreement between both models and the experimental data.

Experiments using the instrument to estimate the parameters of a horizontal ferrous rod buried under a horizontal measurement plane are also described. It was seen that all the location parameters (rod orientation, end locations, depth) of typical reinforcing rod could be estimated with reasonable accuracy at depths of 8 to 18 cm using very simple linear equations. Estimation of rod diameter was unreliable chiefly due to the presence of substantial remnant magnetization.

RÉSUMÉ

On décrit un appareil breveté, portatif qui est le premier capable de repérer des barres parallèles de fer enfouies dans, ou sous un, plan de mesure et ceci, par l'analyse des données du champ magnétique et de la position. L'appareil a plusieurs applications utiles, en particular la détection et la caractérisation des tiges d'acier dans le béton armé.

L'appareil se compose d'un magnétomètre à absorption de flux et d'un détecteur de position montés dans un contenant que l'on manie comme une souris d'ordinateur. Cette souris est reliée à une unité centrale qui contient un micro-ordinateur, un convertisseur analogique-numérique, une unité d'affichage et des piles. Sous la commande du micro-ordinateur, qui contrôle la collecte simultanée des données de la position et du champ magnétique, l'opérateur balaie l'élément de détection sur la surface à mesurer. Par la suite, le micro-ordinateur utilise des algorithmes simples afin d'estimer les paramètres de position, la longueur et le diamètre des tiges.

Ce rapport décrit la version finale de l'appareil. On y present les données expérimentales des champs magnétiques produits par des tiges horizontales et on les compare à des modèles simples d'un cylindre infini et d'un sphéroïde allongé. On a constaté que le rapport entre les modèles et les données expérimentales est très mauvais.

On décrit aussi des essais de l'appareil visant à évaluer les paramètres d'une tige horizontale de fer enfouie sous un plan de mesure horizontal. En utilisant des équations linéaires trés simples, on a découvert que l'on peut mesurer avec assez de certitude tous les paramètres de position (l'orientation, la position des extrémités, la profondeur) et ceci, pour les profondeurs d'enfouissement variant de 8 à 18 cm. À cause de la présence d'une quantité importante de magnétisme résiduel, l'évaluation du diamètre des tiges demeure incertaine.

Executive Summary

There are many applications where a horizontal ferrous rod, rope, pipe or cable lies underneath a smooth planar surface at a constant depth. In such cases one often would like to determine the position and orientation in the plane, the depth of burial and the cross sectional area of the object. Among applications of miltary interest is the identification of the various types of structural concrete members for demolition tasks. Of interest to the miltary and police is the localization and identification of steel or iron pipe bombs. Among civilian applications are the location, mapping and identification of steel or iron conduit buried in floors and walls by the construction industry; the assessment of reinforcing steel in parking garages and buildings; and the location, mapping and determination of diameter of steel gas pipes by gas companies.

There are a number of possible solutions to the problem. Radar and active acoustics have been examined by the nuclear industry to detect steel in concrete shielding walls of nuclear reactors and have shown some success. A solution to the problem which makes use of the fact that the object is ferrous, is to make magnetic field measurements as a function of position on the covering surface and to analyse the data to determine the desired parameters. Unlike acoustics or radar, such a system will not yield false detections from nonferrous inclusions, such as rocks or aggregate. This technique has been used in geophysical exploration and more recently in detection of buried ordnance. Numerous detectors, or magnetometers, are commercially available which can measure small magnetic fields with sufficient sensitivity to detect ferrous rods or pipes with sizes and depths of burial which are typical of the applications mentioned above. The output signals from these detectors are a function of both relative sensor-to-object distance, the object size, shape and orientation. This information cannot be simply separated. To do so, position information must be obtained simultaneously with the magnetic field information and a microprocessor must decode the position and magnetic information to yield object location, orientation and other information. There are a few magnetometer systems which have this ability to collect position and magnetic data but most are designed to locate magnetic anomalies over areas of several thousand square meters. They transfer data to a computer which analyses the data off-line. They can localize a compact ferrous object to within a few times its depth of burial and can classify an object in terms of its rough size. None of them can explicitly determine the location to within a fraction of the depth and explicitly determine the identity of the detected object in real-time. There is also an instrument designed by this laboratory which collects simultaneous magnetic and position data and then uses custom algorithms to locate and identify ferrous compact objects in real-time. It would be of use for the detection of pipe bombs and gas lines, but the cesium vapour sensor used in it makes it too bulky and awkward for the types of small area scans that are necessary to locate reinforcing steel.

This report is concerned with the first problem above, namely the location of reinforcing rod in concrete. A patented hand-held instrument is described that is the first instrument to

explicitly locate ferrous rods parallel to and buried behind or beneath a plane of measurement by analysing magnetic field and position data. It is the result of a concept formulated in 1984 by the Threat Detection Group (TDG) in response to a request by DMilE (then DMER) to investigate ways to characterize reinforcing steel in concrete. The report describes the instrument, developed jointly by TDG and Pylon Electronic Development Ltd., under Task DMER 15.

The instrument consists of a fluxgate magnetometer and position sensor unit enclosed in a small box which is moved by hand somewhat like a computer mouse. The sensor unit is connected by a cable to a processor unit, containing a microprocessor, A/D, displays and batteries. An operator scans the sensor unit over an area on the measurement surface, guided by the microprocessor, while the microprocessor controls the simultaneous collection of magnetic and position data. The microprocessor then uses simple algorithms to estimate the orientation, depth, length and diameter of the rod.

This report also describes research conducted by TDG between 1984 and 1989 to determine ways of calculating location and identification parameters of a ferrous rod from simultaneous position and magnetic field measurements.

Experimental magnetic map data from horizontal rods are presented and compared to two simple models, the infinite cylinder and the long prolate spheroid. It was found that there was very poor agreement between both models and the experimental data.

Experiments using the instrument to estimate the parameters of a horizontal ferrous rod buried under a horizontal measurement plane are also described. It was seen that for rod dimensions and geometries typical of reinforcing rods, all the location parameters, i.e., rod orientation in a horizontal plane, rod end locations (and hence rod length) and rod depth could be estimated with reasonable accuracy at depths of 8 to 18 cm using very simple linear equations. Estimation of rod diameter was not possible with any degree of reliability chiefly due to the presence of substantial remnant magnetization.

Although the instrument represents a significant advance in ferrous rod location and identification technology, more research is necessary to develop a practical instrument. Future experiments and improvements to the detector are discussed.

ACKNOWLEDGEMENT

John McFee, Robert Ellingson and Yogadhish Das are with the Threat Detection Group, Mobility Systems Section, Defence Research Establishment Suffield. John Elliott is with Pylon Electronic Development Ltd., Ottawa.

Malcolm Bell, formerly with TDG, played an integral part in the early part of the project by specifying the Brown sensor as the preferred magnetometer and by constructing preliminary magnetometer sensors and circuits.

Richard Pinnell, formerly with TDG, breadboarded the first interface between the microprocessor and the position encoder and magnetometer.

The authors would like to thank Glen Thurston and Ian Johnson who were Research Assistants in the Threat Detection Group during the summers of 1986 and 1989 respectively and assisted in the collection and processing of much of the data presented in this report.

The authors are grateful to Gord Briosi and Al Carruthers for providing much useful information on reinforced concrete.

This work was jointly supported under Chief Research and Development Project Number 031SD and under Task DMER-15 (Project Number 27B77).

Table of Contents

List of Figures

List of Tables

1. Introduction

There are many applications where a horizontal ferrous rod, rope, pipe or cable lies underneath a smooth planar surface at a constant depth. In such cases one often would like to determine the position and orientation in the plane, the depth of burial and the cross sectional area of the object. Among applications of military interest is the identification of the various types of structural concrete members for demolition tasks. Since all tensile loads must be carried by the steel present, usually in the form of bars, rods or wire rope or cable, explosive demolition relies on attacking the steel or places where it is absent. Knowledge of the size, depth of burial, and orientation of the steel rods (often called "rebar") is crucial for a successful demolition using a minimum of explosives. Also of interest to the military and police is the localization and identification of steel or iron pipe bombs. Such information could distinguish between conduit and bombs in a floor, wall or culvert and give an estimate of the size of the bomb. Among civilian applications is the location, mapping and identification of steel or iron conduit buried in floors and walls by the construction industry. Such information can save costly dismantling of walls or floors in order to find specific conduit. Another important application is the assessment of reinforcing steel in parking garages and buildings, both to assess corrosion and to determine if installation was done according to specifications [1]. Gas companies are continually presented with the problem of locating, mapping and determining diameter of steel gas pipes. Accurate location and identification can substantially reduce digging costs.

There are a number of possible solutions to the problem. Radar and active acoustics have been examined by the nuclear industry to detect steel in concrete shielding walls of nuclear reactors and have shown some success. A solution to the problem which makes use of the fact that the object is ferrous, is to make magnetic field measurements as a function of position on the covering surface and to analyse the data to determine the desired parameters. Unlike acoustics or radar, such a system will not yield false detections from nonferrous inclusions, such as rocks or aggregate. This technique has been used in geophysical exploration and more recently in detection of buried ordnance [2]. Numerous detectors, or magnetometers, are commercially available which can measure small magnetic fields with sufficient sensitivity to detect ferrous rods or pipes with sizes and depths of burial which are typical of the applications mentioned above. The output signals from these

detectors are a function of both relative sensor-to-object distance, the object size, shape and orientation. This information cannot be simply separated. To do so, position information must be obtained simultaneously with the magnetic field information and a microprocessor must decode the position and magnetic information to yield object location, orientation and other information. There are a few magnetometer systems which have this ability to collect position and magnetic data but most are designed to locate magnetic anomalies over areas of several thousand square meters. They transfer data to a computer which analyses the data off-line. Some claim to be able to localize a compact ferrous object to within a fraction of its depth of burial and they can classify an object in terms of its rough size. None of them can explicitly determine the location to within a fraction of the depth and explicitly determine the identity of the detected object in real-time. There is also an instrument designed by this laboratory [3] which collects simultaneous magnetic and position data and then uses custom algorithms to locate and identify ferrous compact objects in real-time. It would be useful for the detection of pipe bombs and gas lines, but the cesium vapour sensor in it makes it too bulky and awkward for the types of small area scans that are necessary to locate reinforcing steel.

This report is specifically concerned with the first problem above, namely the location of reinforcing rod in concrete. In 1984 the Threat Detection Group (TDG), then the Ordnance Detection Group, at the Defence Research Establishment Suffield (DRES) was asked by D Mil E (then DMER) whether it was possible to develop an instrument which could distinguish between reinforced and prestressed/post-tensioned concrete. In response, TDG constructed a rudimentary hand-held magnetometer sensor package and carried out measurements on reinforced concrete to determine the feasiblity of using a magnetic sensor in such a role. The results were encouraging [4] and a Task DMER 15 was initiated in April 1985 with the aim "to develop a detector which will locate reinforcing steel reliably in concrete to a maximum depth of 30 cm and indicate the rebar diameter". Based on the previous research, an instrument was proposed that would simultaneously collect , under microprocessor control, magnetic and positional information (position coordinates) in a plane of measurement behind or beneath which the steel rod was buried. The microprocessor would then apply various algorithms to the data. The instrument would consist of a magnetometer and position sensor enclosed in a small box which would move somewhat like a computer mouse. The mouse was connected to a microprocessor unit by a cable. An operator would scan the mouse over an area of the concrete surface, guided by the microprocessor. Afterwards, the microprocessor would estimate the orientation, depth, position, length and diameter of the rod.

A breadboard model of the rebar detector was completed by TDG in the spring of 1985 and a contract was awarded to Pylon Electronic Development Ltd., Ottawa, to manufacture two exploratory development models from the TDG design. The detectors were received by TDG in the autumn of 1985. DRES conducted tests and made a number of modifications throughout 1986. These tests revealed that there were a number of problems with the mouse which combined to make the mouse difficult to move smoothly and to prevent repeatable results from being obtained. Pylon incorporated DRES suggestions and by March 1987

manufactured two improved mice [5]. DRES conducted experiments to test the instrument's performance, revealing a number of new problems which were solved. Experiments continued until autumn 1989 to determine the accuracy and overall performance of the modified rebar detector and methodology for location and identification of long steel rods which simulate reinforcing rods. A U.S. patent for the instrument and the method of locating and identifying ferrous rods and compact objects by analysis of simultaneous position and magnetic field measurements was awarded in 1989 [6] and a Canadian patent in 1990 [7].

This report describes the final version of the instrument designed to locate reinforcing rods in concrete. The experiments using the final version of the instrument which were performed to quantify its performance are also described.

2. Theory

2.1 Magnetic Field Measurement

Reinforcing rods can be characterized as mild steel or soft iron rods with diameters typically between 0.64 cm (1/4 inch) and 1.90 cm (3/4 inch) and with varying lengths of up to roughly 2 m. The depth of the rod below the concrete surface varies from one structure to another but is frequently between 3.8 cm (1.5 inches) and 20.3 cm (8 inches). This implies that the spatial extent of the measureable magnetic fields associated with such rods is generally less than 1 m in width and 4 m in length. Peak fields vary from a few hundred nT (nanoTeslas) to ten thousand nT, depending on the depth, and the time taken to measure such fields is a few minutes. The earth's field is constant over such distances (magnetic induction gradient $\sim$ 10 nT/km) and does not change significantly during this time. In spite of occasional field nonuniformities arising from local magnetic phenomena, one can in practice usually assume that the ambient field is constant [8].

There are two types of magnetometer - vector sensors and total field sensors. The former measures the magnetic field along a particular direction (the sensitive axis) and includes fluxgate magnetometers, such as the one used in the present work. Fluxgate magnetometers can be small, inexpensive and reliable but the signal output of a vector magnetometer is sensitive to small changes in the orientation of the sensor. In the present work, because the measurement surface is very flat and smooth, this orientation sensitivity can be kept reasonably small. For example, if the secondary field (field due to the rod) in a cartesian coordinate system is denoted by $\vec{B} = (B_1, B_2, B_3)^T$, where the superscript T denotes the transpose and if the primary (ambient, i.e., earth's) field is $\vec{B}_0 = (B_{01}, B_{02}, B_{03})^T$, then a vector magnetometer oriented along the j axis, where $j = 1, 2, 3$, would measure

$$B_{vj} = B_{0j} + B_j \ . \tag{2.1}$$

In the experiments described in this report, the cartesian system is aligned so that the B_3 component is vertical and the B_1 component lies along the direction of travel of the magnetometer sensor (east-west). The ambient field at the location of our laboratory is roughly 60000 nT and is tilted 17° degrees from the vertical. A vertically oriented vector sensor will measure a field of $60000 \cos 17° = 57378.3$ nT at rest. If while moving, the sensitive axis tilts from the vertical by 0.1° in the plane of the earth's field vector (north-south direction), the measured field will vary by ± 30.6 nT. This is because the tilted sensor

measures less of the vertical component of the ambient field ($\propto \cos\theta_s$ where θ_s is the angle between the vertical and the sensitive axis) and more of the horizontal component ($\propto \sin\theta_s$). The deviation is dominated by the sine term and so the latter is a worst case estimate. If the sensor tilts only in the east-west plane, the horizontal component of the earth's field is not detected and so the measured field will vary by ± 0.1 nT.

Principles of operation of fluxgate magnetometers and low noise magnetic measurement techniques may be found in [8].

2.2 Magnetic Field of an Infinitely Long Cylinder

This section presents the first of two simple mathematical models chosen for comparison with experimental magnetic field data. A solid cylindrical ferrous rod of infinite length is assumed to lie in air in a static uniform ambient magnetic field. The symmetry axis of the rod is assumed to be horizontal. The rod has no remnant magnetization. A three dimensional cartesian coordinate system whose origin coincides with the center of the rod is defined. The 3 component of an arbitrary vector $\vec{A} = (A_1, A_2, A_3)^T$ in this system is oriented in the vertical direction and the 2 component lies in the direction of the symmetry axis of the rod. The direction parallel to the 2-axis is referred to as the longitudinal direction and that parallel to the 1-axis is called the transverse direction. If θ is the angle between the 3 axis and the earth's field vector and ϕ is the angle between the 1 axis and the projection of the earth's field vector on the horizontal plane, then the vertical component of the magnetic field at a point (x_1, x_3) in space is given by [9]

$$B_3 = \frac{2G}{\left[x_1^2 + x_3^2\right]^2}\left(B_{01}x_1x_3 + B_{03}\left[x_3^2 - x_1^2\right]\right) \tag{2.2}$$

where B_{01}, B_{03} are the components of the earth's field given by

$$B_{01} = B_0 \sin\theta_0 \sin\phi_0 \tag{2.3}$$

$$B_{03} = B_0 \cos\theta_0 \tag{2.4}$$

and G is a constant for a given rod which is a function of the diameter of the rod d and the relative permeability of the rod μ_r

$$G = \frac{d^2}{4}\frac{\mu_r - 1}{\mu_r + 1} \ . \tag{2.5}$$

It is assumed that the sensor measuring B_3 is restricted to move in the transverse direction. If $x_3 = z$ is the constant depth (distance from the plane of motion of the center of the magnetic sensor to the center of the rod), the variation of B_3 as a function of x_1 may be analyzed using the above equations. This gives expressions for z and d of the rod

$$z = 0.9717x_{1/2} \tag{2.6}$$

$$d = z\sqrt{\pi \frac{B_3^{max}}{B_{03}}} \tag{2.7}$$

where $x_{1/2}$ is the full width at half maximum (FWHM) and B_3^{max} is the maximum value of B_3 along the direction of sensor motion. The transverse (x_1) position of the field maximum, x_{1m}, is found by differentiating Equation 2.2 with respect to x_1 and setting the resulting expression equal to 0. This gives

$$2B_{03}x_{1m}^3 - 3B_{01}zx_{1m}^2 - 6B_{03}z^2x_{1m} + B_{01}z^3 = 0. \tag{2.8}$$

The model should be a reasonable approximation to experimental data corresponding to the same geometry, provided that the rod has no remnant magnetization, that the diameter of the rod and the depth are both much less than the length of the rod and that measurements are made far from the ends of the rod (compared to its length).

2.3 The Magnetic Field of a Long, Horizontal Prolate Spheroid

In this section, we present the second of two simple mathematical models chosen for comparison with experimental magnetic field data. The model is of the magnetic field induced in a homogeneous long, horizontal prolate spheroid by a uniform magnetostatic field in air. The model, generalized to arbitrary spheroid size, shape and orientation has been shown to provide magnetic fields that are a good approximation to those of real spheroids and some unexploded ordnance in the earth's field [10], [11]. Since a long thin prolate spheroid looks somewhat like a long rod, it is reasonable to think that the induced fields of the two may be similar. A detailed derivation of the generalized model may be found in [8].

It is assumed that a homogeneous uniformly permeable spheroid, with magnetic permeability $\mu_r\mu_0$ and no permanent magnetization, sits in a homogeneous surrounding medium with permeability μ_0, where μ_0 is the permeability of free space. There exists a uniform parallel external magnetostatic field. A cartesian coordinate system whose 2-axis coincides with the symmetry axis of the spheroid, has a vertical 3-axis and an origin at the geometric center of the spheroid. By carrying out a multipole expansion of the static field, and with the assumptions of uniform parallel internal magnetization, it may be shown that the secondary induced magnetic induction measured at a point $\vec{R} = (X_1, X_2, X_3)$ in free space, complete to fourth order, is given by [8]

$$\vec{B} = \vec{B^{(2)}} + \vec{B^{(8)}} \tag{2.9}$$

where $\vec{B^{(2)}}$ is a dipole field term and $\vec{B^{(8)}}$ is an octupole field term. The two field terms may be expressed in component notation using summation convention as

$$B_\alpha^{(2)} = \frac{\mu_0}{4\pi} R^{-3}\left(-M_\alpha^{(1)} + 3R^{-2}\left[X_\beta M_\beta^{(1)}\right]X_\alpha\right) \tag{2.10}$$

and

$$B_\alpha^{(8)} = \frac{\mu_0}{8\pi} R^{-5}\left(3M_{\alpha\beta\beta}^{(3)} - 15R^{-2}\left[X_\alpha X_\beta M_{\beta\gamma\gamma}^{(3)} + X_\beta X_\gamma M_{\alpha\beta\gamma}^{(3)}\right] + 35R^{-4}X_\alpha X_\beta X_\gamma X_\delta M_{\beta\gamma\delta}^{(3)}\right) \tag{2.11}$$

where $M_\alpha^{(1)}$ is a component of the dipole moment vector, and $M_{\alpha\beta\gamma}^{(3)}$ is a component of the rank 3 octupole moment tensor.

The dipole moment is given by

$$M_\alpha^{(1)} = M'_\alpha V' \quad \alpha = 1,2,3 \tag{2.12}$$

where V' is the spheroid volume. For the octupole moment tensor, there are only 6 independent elements. These are

$$M_{111}^{(3)} = 3M_{331}^{(3)} = 3M'_1 I_{11} \;;\; M_{333}^{(3)} = 3M_{113}^{(3)} = 3M'_3 I_{11} \;;\; M_{222}^{(3)} = 3M'_2 I_{22}$$

$$M_{112}^{(3)} = M_{332}^{(3)} = M'_2 I_{11} \;;\; M_{221}^{(3)} = M'_1 I_{22} \;;\; M_{223}^{(3)} = M'_3 I_{22} \tag{2.13}$$

For a prolate spheroid whose symmetry axis length is $2ae$ ($e > 1$) and whose maximum diameter orthogonal to the symmetry axis is $2a$,

$$V' = \frac{4}{3}\pi e a^3 \;;\; I_{11} = \frac{4\pi}{15} e a^5 \;;\; I_{22} = \frac{4\pi}{15} e^3 a^5 \;. \tag{2.14}$$

Note also that

$$M_{\alpha\alpha\beta}^{(3)} = M_{\alpha\beta\alpha}^{(3)} = M_{\beta\alpha\alpha}^{(3)} \tag{2.15}$$

$$M_{\alpha\beta\gamma}^{(3)} = 0 \quad \text{if} \quad \alpha \neq \beta \neq \gamma \neq \alpha \;. \tag{2.16}$$

Assume that the external magnetic field (usually the earth's) in the absence of the spheroid is $\vec{B}_0 = (B_{01}, B_{02}, B_{03})^T$. The magnetization is given by

$$M'_j = \mu_0^{-1} F_j B_{0j} \quad j = 1,2,3 \tag{2.17}$$

The demagnetization factors F_j for $e \gg 1$ are given by

$$F_1 = F_3 \approx 2 \tag{2.18}$$

$$F_2 \approx \frac{1}{\frac{1}{\mu_r - 1} + \frac{\ln(2e) - 1}{e^2}} \tag{2.19}$$

In our case $75 < e < 170$, making the approximations for F_j valid to within less than 1%.

Equations 2.9 through 2.19 allow one to calculate the magnetic field $\vec{B}$ at a point in space due to the presence of the spheroid, given the size and shape of the spheroid (a, e), the magnetic material properties of the spheroid (μ_r), and the magnitude and direction of the earth's magnetic field (B_0, θ_0, ϕ_0). Equation 2.19 is not strongly dependent on μ_r for $\mu_r \gg 1$. For all model calculations done in this study, μ_r has been set equal to 1000, which ia a typical value encountered in practice.

When using the spheroid equations to model long rods, one must determine the parameters a and e from the rod diameter d and length l. This is not a trivial exercise, since there is no simple relationship between these parameters. We have chosen to equate the

spheroid volume $V_{spheroid}$ to the rod volume V_{rod} in order to attempt to make the spheroid dipole moment equal that of the rod. (in fact, this will only be an approximation, since the magnetization in the two objects is not the same.) With the constant volume assumption, there are still two reasonable choices. We can use a constant length approximation

$$a = \sqrt{\frac{3}{8}}d \tag{2.20}$$

$$e = \sqrt{\frac{2}{3}}\frac{l}{d}$$

or a constant diameter approximation

$$a = \frac{1}{2}d \tag{2.21}$$

$$e = \frac{3}{2}\frac{l}{d}$$

where for both

$$V_{spheroid} = V_{rod} \quad .$$

Both approximations were applied to a number of different rod diameters, depths and lengths used in the experiments described in this report. There were slight differences between the two approximations, but these were small compared to the differences between model and experimental results and the variability between rods.

2.4 Remnant Magnetization

The two previous models assume that the magnetization of the rods is due solely to that which is induced by the ambient field. In practice, ferrous objects may also have remnant or permanent magnetization which is a function of the metallurgical properties of the object as well as its thermal, mechanical and geomagnetic history. Remnant magnetization is very difficult to model since its strength and direction are often unknown for an individual object and may vary from object to object of the same shape and size. Remnant magnetization is fixed to the body of the object so that if the body is rotated through a given angle, the distribution of remnant magnetization also rotates by the same angle. This provides a simple test for remnant magnetization in a horizontal ferrous rod. When a rod is rotated 180° about a vertical axis, the magnetic field map will be identical to that of the unrotated rod if the magnetization is purely induced. If the remnant magnetization is much larger than the induced magnetization, the magnetic field map of the rotated rod can be obtained by rotating the map of the unrotated rod by 180° about a vertical axis. If the induced and remnant magnetizations are comparable, then the rotated and unrotated fields will differ, but not in a simple fashion.

3. Experimental Method

3.1 The DRES/Pylon Rebar Detector

To obtain magnetic data as a function of position in the plane over a horizontal ferrous rod, a novel instrument was developed. The DRES/Pylon rebar detector collects simultaneous magnetic and position data and can be used to estimate rod position and dimensions. A rudimentary instrument [4] was used to prove the concept, but it had no automatic position determination, poor magnetic sensitivity and stability and it was difficult to operate. The instrument used in this study was designed and constructed by Pylon Electronic Development Ltd. [5] based on a patented [6], [7] DRES conceptual design. The detector consists of two units, a sensor unit and a processing unit, which are connected by a flexible cable which passes electrical signals and power. The instrument with an early version of the sensor unit is shown in Fig. 3.1. The sensor unit used in the present study appears very similar to that of the photograph except that it lacks the LCD display, the connecting cable is thinner, and it has a variable gain knob for the magnetometer amplifier.

The sensor unit was initially dubbed a mouse because of its similarity to a computer mouse. Because of its larger size, however, (18 cm $\times$ 4.5 cm $\times$ 5 cm), it was soon renamed the "Rebar Rat". It houses a single axis vector magnetometer with associated signal conditioning circuitry and a position sensor which measures linear displacement along the short horizontal axis (assuming the unit is sitting on a horizontal surface). Total field magnetometers and two-axis position measuring systems were considered in the initial concept [6], [7] but were deemed too complicated for the first prototype. A Brown solenoidal ultra-low power fluxgate magnetometer with associated drive and sense circuits [12], [13] was chosen because of its low power, small size, good stability and high sensitivity. The magnetometer is AC coupled to the rest of the signal processing chain, which eliminates the comparatively large DC offset due to the earth's magnetic field. The nominal bandpass filter cutoffs are 0.1 Hz and 10 Hz. Because the AC coupling time constant is approximately 10 seconds, a fast zero button has been included to speed up initial measurements. Three gain settings of 1, 10, 100 nT/ADC count are selectable. This increases the dynamic range of the magnetic anomaly measurements. The position sensor consists of a rotating wheel connected to an optical shaft encoder by means of a pulley arrangement, with additional wheels on the underside of the unit to provide stability. The magnetometer amplifier gain switch, a "Mode" button to step through the menu of the microprocessor progam and the

fast zero button are located on the top of the sensor unit.

The processing unit contains an 8-bit analog to digital converter (ADC), bar graph and digital LCD displays with associated electronics and a Motorola 6805 microprocessor. As well, lithium batteries which power the instrument are contained in this unit. A block diagram is shown in Fig. 3.2.

In operation, the magnetometer and position sensors provide magnetic field values with the corresponding position coordinates in the plane of measurement as the sensor housing is moved about on the surface under which the ferrous rod is buried. The magnetometer and signal conditioning circuitry produce an analog signal which is digitized by the ADC. The position encoder produces a digital pulse train which is read by a parallel input/output port of the microprocessor. The microprocessor controls the digitization and storage of magnetic field values. It also controls the counting and phase measurement of the position encoder pulse trains (the latter allows forward and backward motion to be distinguished) and converts that information to a displacement reading. The microprocessor also directs the actions of the operator and controls execution of the algorithms necessary to calculate location and dimensions of the ferrous rod from the magnetic and position data. The algorithms and control program are stored on erasable programmable read only memory (EPROM) and the data are stored in random access memory (RAM). Magnetic field values may be displayed as either a bar graph whose length increases with increasing field value, a digital number, or an audio tone which increases in frequency as the field values increase. All displays and the audio output are controlled by the parallel output ports of the microprocessor.

The menu-driven software has the following modes which are selected using the "Mode" button on the sensor unit.

- Search - This mode is automatically entered after pressing the "Reset" button on the side of the instrument. A bar graph indicates field strength so that the operator can scan an area to look for magnetic field values of sufficient strength and spatial extent to warrant further investigation. This mode can be used to mark local magnetic field maxima in order to determine the orientation in a horizontal plane of the rod.

- Depth - This mode is entered by pressing the Mode button in Search mode. The operator selects a line at right angles to the line of field maxima. The sensor unit is moved along the line until it is well past the field maximum. The program signals the operator to stop. The depth of the rod is then estimated using the simple formula for an infinite length cylinder (Section 2.2, Equation 2.6) and displayed.

- Area - This mode is entered by pressing the Mode button in Depth mode. The program tells the operator to move the sensor unit backward along the scan line until it is directly over the field maximum. The operator is told to stop and the cross sectional area of the rod is estimated, using the simple formula for an infinite length cylinder (Section 2.2 Equation 2.7), and displayed.

The two prototype detectors, as delivered, had a number of problems. First, distance

measurement was not repeatable. This was caused by the slow speed of the simple, low cost microprocessor that had been chosen and was corrected by software modifications. Second, the magnetic field signal-to-noise ratio was much poorer than that theoretically achievable from the sensor. Noise was due to excess vibration when the sensor unit moved, magnetic fields from rotating steel parts in the optical encoder and associated shafts and excess noise in the amplifier/filter circuit. The first component was decreased by addition of a skid plate to the underside of the sensor unit. The second was reduced by replacing some steel parts in the optical encoders and degaussing the remaining steel components. A new low noise amplifier/filter circuit was designed to replace the existing one. Overall, the signal-to-noise ratio was improved by a factor greater than 10. There were also some errors in the control software that were corrected and some modifications were made to the software to improve performance.

These changes substantially improved performance, but there were more fundamental problems that required major changes. The original sensor unit was made of aluminum, which made it quite heavy. Because a bar graph display was put on the sensor unit, the connecting cable was thick and not very flexible. The configuration of support wheels also made the unit unstable. There was a need for selectable gain on the amplifier electronics and some changes to the amplifier/filter board. Finally, parts of the encoder and drive shafts had steel components that still caused excessive periodic magnetic noise. All these flaws combined to make it difficult to move the unit smoothly and also prevented precise measurements from being obtained. Based on suggestions from DRES, Pylon manufactured two improved sensor units with Delrin plastic cases. The display was removed and hence a much thinner cable was employed. A more stable wheel configuration was implemented and steel encoder parts were replaced with nonferrous components.

These units, although much improved, revealed a new set of problems that had been masked by the poor precision of the old unit. Examination revealed the presence of periodic magnetic noise with a fundamental frequency corresponding to that of the drive wheels (Fig. 3.3). The typical noise standard deviation was 28.5 nT. Further examination revealed that the noise was indirectly caused by turning of the optical encoder's nonferrous drive shaft. Static charge which could not leak through the Delrin case, would build up inside the case. As the shaft rotated, the plastic base plate holding it would flex, causing a periodic change in capacitance. The base plate was replaced with one made of 1.5875 mm thick aluminum to provide rigidity and to allow charge to dissipate. An example of the noise inherent in moving the improved sensor unit after final modifications is shown in Fig. 3.4. The typical standard deviation dropped to 15.2 nT. This should be compared with the magnetic noise from a stationary sensor unit (Fig. 3.5). Ten separate two second long magnetic field measurements were taken over a period of several minutes with a stationary sensor unit to characterize the background noise of the magnetometer. The average DC shift was 1.07 ± 0.95 nT and the average standard deviation was 0.53 ± 0.19 nT. Clearly then, the bulk of the detector noise is motion noise.

3.2 Experimental Layout

Measurements were made in the Threat Detection Group's nonmetallic laboratory which has been described in detail in [10]. The laboratory is a 12 m diameter hemispherical nonmetallic building with minimal metal content. Magnetic field gradients were typically no greater than 1 or 2 nT/m in the usable portions of the building. Magnetic field fluctuations were limited by geomagnetic noise and were typically $\pm$1-2 nT/hour during the time of day in which measurements were made (mid-morning, afternoon). In the time necessary to measure a magnetic field map ($\sim$15 minutes or less), background noise fluctuations were less than the minimum quantization error of magnetic data received by the microprocessor (1 nT) and thus no reference magnetometer was used for background subtraction. The experimental set-up is shown schematically in Fig 3.6.

The measurement table on which the magnetometer moves was situated in a low gradient part of the laboratory. The table was made of wood with brass screws and was sufficiently sturdy to ensure negligible displacement of the measurement surface when the rebar detector was moved on it. To ensure repeatable placement, a ferrous rod was placed in a "V" notch of a horizontal wooden rod holder, situated under the table. A wooden guide was attached to the measurement surface at right angles to the rod direction. The horizontal measurement surface measured 0.74 m in the direction of the rod, 1.25 m in the guide direction direction and was 0.52 m above the floor. The table was oriented so that the long axis of the guide was in an east-west direction.

A separate wooden table, on which the electronics was placed, was situated roughly 1 m from the measurement table. This ensured that stray magnetic fields from the large electronic components, such as the computer and logic analyser, would not interfere with the magnetometer sensor.

One aim of the experiments was to collect complete magnetic field maps in order to determine optimum algorithms for estimation of rod parameters. The microprocessor, however, did not have sufficient resources to be able to store a complete map. To do so, the microprocessor of the rebar processor unit was connected via a dip connector to the logic analyser. The latter was programmed so that it would capture data written to the address block in memory where magnetometer data was stored. This data, in turn was downloaded to the laptop computer where it could be concatenated into a magnetic map and plotted.

3.3 Procedure

To collect a magnetic map the following procedure was used. Initial experiments had shown that the magnetic noise and drift became stable about 2 to 3 minutes after power-up. Thus, before collecting the initial map, the electronics were connected and powered up for at least five minutes. The logic analyser was programmed as described above. The operator removed all metal and placed it far from the measurement table. The rod was placed in the rod holder so that it was horizontal with its symmetry axis pointing in a north-south

direction. Each bar had previously been marked with a line every 5.0 cm along its length. The marks were numbered so that the two ends of the rod could be distinguished from one another. The set of position and magnetic data collected along the guide direction is called a "magnetic scan" or a "scan line". For each scan line, the rebar sensor unit was placed at a marked start position near the western (leftmost) side of the measurement table. The northern face of the unit was placed flush against the guide. The rebar detector program was started by pressing the reset button on the processor unit and pressing the mode button to advance the program to the "Depth" mode. The logic analyser was armed. The sensor unit was moved from west to east, keeping the northern face flush against the guide, until the operator was signalled to stop by the logic analyser. The rate at which magnetic data was captured was programmable. Typically a magnetic value was obtained every 0.5 cm until 250 values had been stored. Magnetic data were transferred to the lap top hard disk for permanent storage. The operator then set the sensor unit at the start position. The rod was moved southward in the rod holder until its next mark was in line with the table mark and another scan was obtained. The procedure for obtaining a scan line was repeated until a complete two dimensional distribution of the magnetic field of the rod, called a "magnetic map", had been obtained. This typically consisted of 40 scan lines with a 5.0 cm spacing. The position along the guide is called the transverse position and the position along the rod axis is called the longitudinal position. The zero transverse position corresponds to the magnetometer being directly above the symmetry axis of the rod. The data could be displayed on the laptop computer and the procedure could be repeated for a new magnetic map.

3.4 Initial Experiments

Prior to commencing the location and identification experiments, a number of magnetic maps were collected to optimize operational procedures and parameters.

Optimum scanning speed for the sensor was first determined. Problems with DC shifts and nonstochastic noise were noticed when the sensor unit was moved too quickly. If the sensor was moved too slowly, the low frequency cutoff of the magnetometer filter prevented variations in the magnetic field from being passed to the ADC. A speed of 30 to 40 cm/second was found to be optimum and readily achievable. All maps used for analysis were collected at that speed which corresponds to a traverse time of 3 to 4 seconds across the table.

An example of a magnetic field map is shown in Fig 3.7. The rod is a 1.27 cm diameter 143.0 cm long mild steel rod at a depth of 13.0 cm. The difference between two maps of the same rod at the same depth serves to illustrate the degree of repeatability and the sources of error in the measurements (Fig. 3.8). The two maps used to form the difference were of a 1.27 cm diameter 143.0 cm long mild steel rod (rod h1) at a depth of 13.0 cm. The mean difference between the two maps is 0.2 nT and the standard deviation is 23.4 nT.

There are a number of possible sources of error in the magnetic field maps. These may

be grouped in the following manner:

1. Magnetometer Sensitive Axis Roll - A rotation of the magnetometer sensitive axis about the north-south axis will cause a fluctuation in the measured magnetic value which is proportional to the cosine of the angle of rotation as explained in Section 2.1. As previously noted, the typical standard deviation of the moving sensor with no rod present was approximately 15 nT. This corresponds to roll angle variation with a standard deviation of approximately 1.2°, assuming that the entire error is due to roll. Since the sensor unit width is approximately 5.1 cm, this corresponds to vertical deviations with a standard deviation of 0.1 cm across the width of the sensor unit. Given the experimental method and instrument tolerances, this seems to be reasonable.

2. Magnetometer Sensitive Axis Pitch - A rotation of the magnetometer sensitive axis about the east-west axis will cause a fluctuation in the measured magnetic value which is proportional to the sine of the angle of rotation as explained in Section 2.1. Since the sine function varies faster than the cosine for small angles, this would be the dominant term if pitch and roll angles were similar. However, by moving the sensor unit in an east-west direction against the measurement table guide, the pitch becomes negligible.

3. Magnetometer Sensitive Axis Yaw - A rotation of the magnetometer sensitive axis about the vertical axis will cause a fluctuation in the measured magnetic value if the sensitive axis is not completely vertical. However, the sensor unit is constrained by the guide along which it moves, so that this error is negligible.

4. Position Measurement System Uncertainty - This includes cumulative errors due to the position encoder, all wheels and pulleys that connect to it and the software which reads the encoder value. Repeated measurements on a precisely measured track have shown that the standard deviation of the positional uncertainty is approximately 2 mm.

5. Slope Error - Positional uncertainty chiefly manifests itself as an apparent magnetic error term when examining the difference of two magnetic maps of the same object and geometry to determine map measurement repeatability. The standard deviation of the magnetic error σ_{B_3} is given by

$$\sigma_{B_3}^2 = \left(\frac{\partial B_3}{\partial x}\right)^2 \sigma_x^2 \tag{3.1}$$

where σ_x is the standard deviation of the positional uncertainty, and x is the transverse position. This assumes a negligible positional error in the vertical and longitudinal directions. For the case of Fig. 3.8, the maximum transverse magnetic gradient is $\approx$ 80 nT/cm (Fig. 3.7) which gives $\sigma_{B_3} \approx$ 16 nT. Gradients near the maximum will occur when estimating the full width at half maximum. When measuring peak magnetic field values, this error is negligible since the gradient is nearly zero. The error will also be larger for shallower rods which have higher gradients.

6. Magnetic Measurement Uncertainty - This includes the DC offset, linearity, stability and sensitivity of the magnetometer, signal conditioning circuit and ADC. As stated previously, measurements show that the DC offset and sensitivity of the entire magnetometer signal processing chain is approximately equal to the least count of the ADC at the highest gain setting (1 nT). At lower gain settings, the error is determined by the least count of the ADC (10 nT or 100 nT). Stability error is essentially negligible, chiefly due to the AC coupling.

If we assume that the various error terms are statistically independent, the variance of the total error σ_{tot}^2 is equal to the sum of the variances of the individual terms, i.e.,

$$\sigma_{tot}^2 = \sigma_{roll}^2 + \sigma_{magn}^2 + \sigma_{slope}^2 \tag{3.2}$$

where σ_{roll}^2, σ_{magn}^2, σ_{slope}^2 are the respective variances due to magnetometer roll, magnetic measurement uncertainty and slope error. If slope error is negligible, i.e., if no rod is present or measurements are made near field maxima or far from the rod, $\sigma_{tot} \approx 15$ nT. For the maximum slope portion of Fig. 3.7, $\sigma_{tot} \approx 22$ nT. As seen previously, both values are consistent with what has been measured.

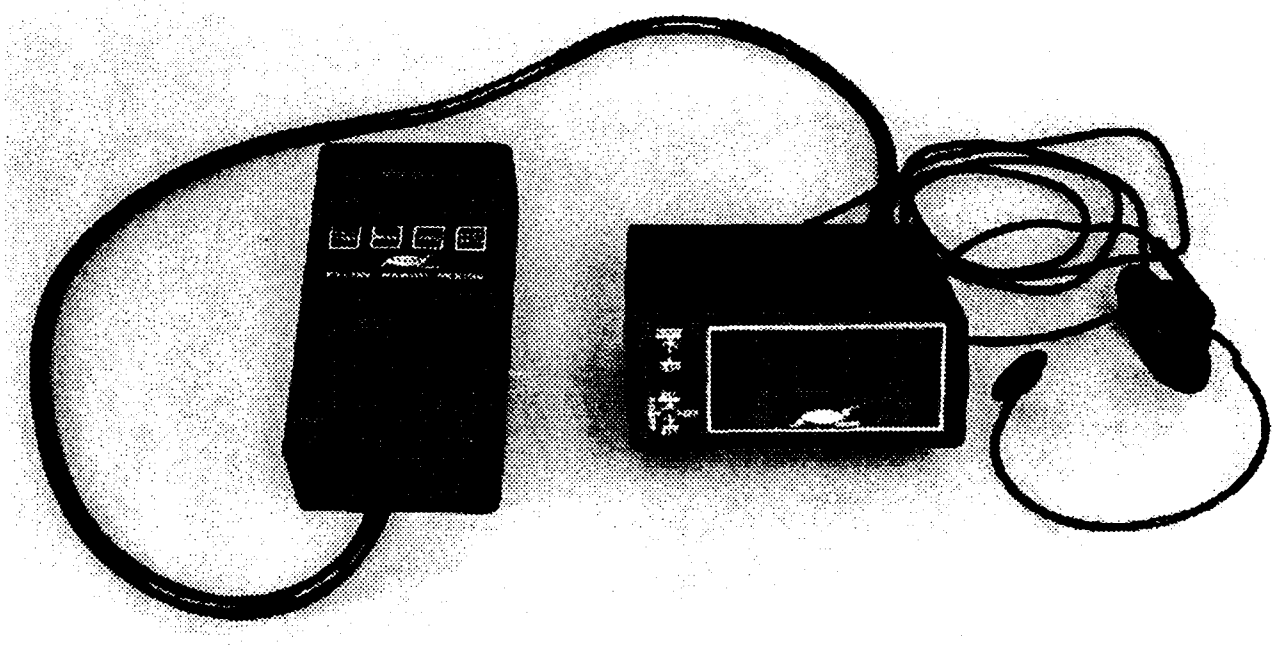

Figure 3.1

DRES rebar detector. The sensor unit or mouse containing the magnetometer and position sensor is on the left. At center is the processing unit which contains the microprocessor board. Headphones are on the right.

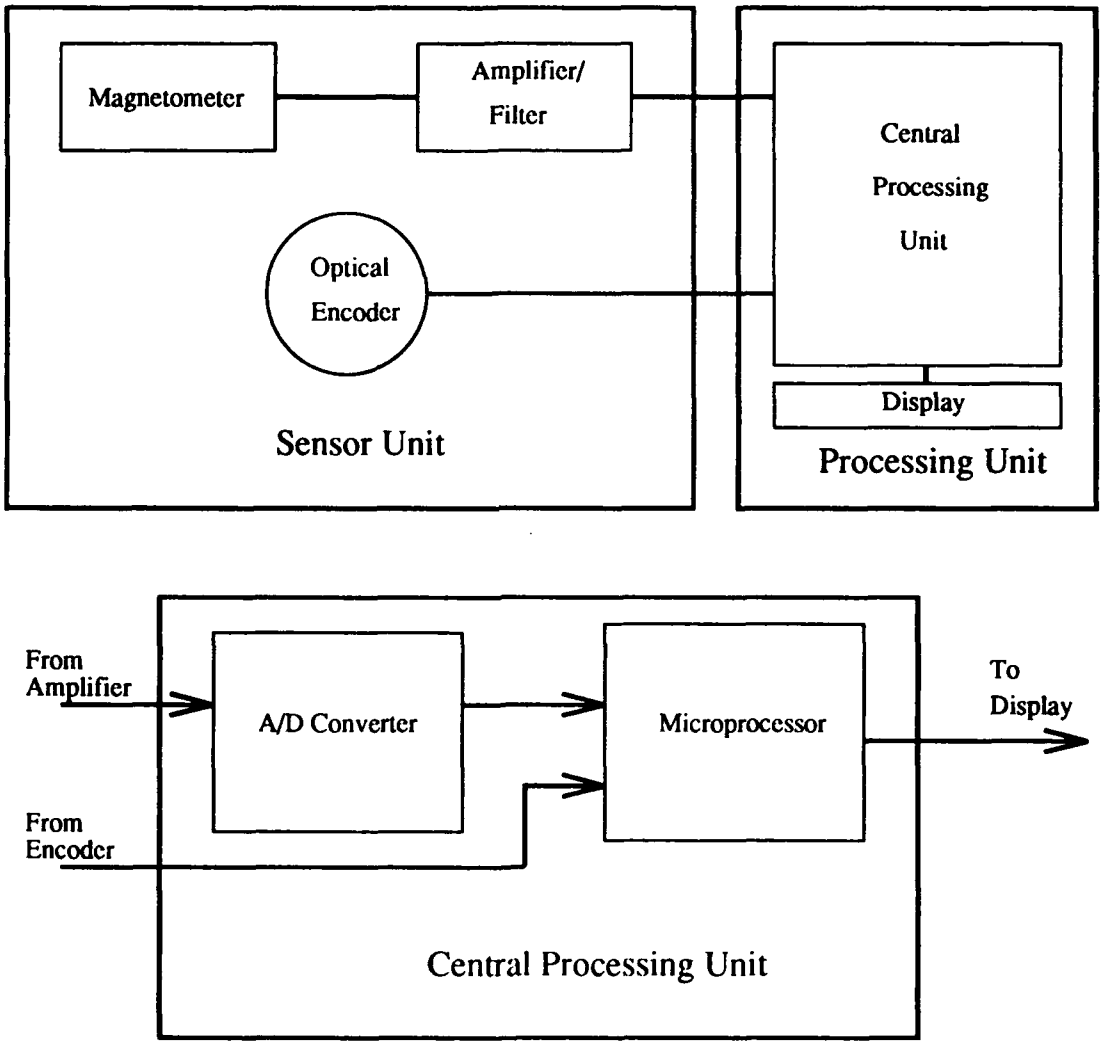

Figure 3.2

DRES rebar detector electronic block diagram.

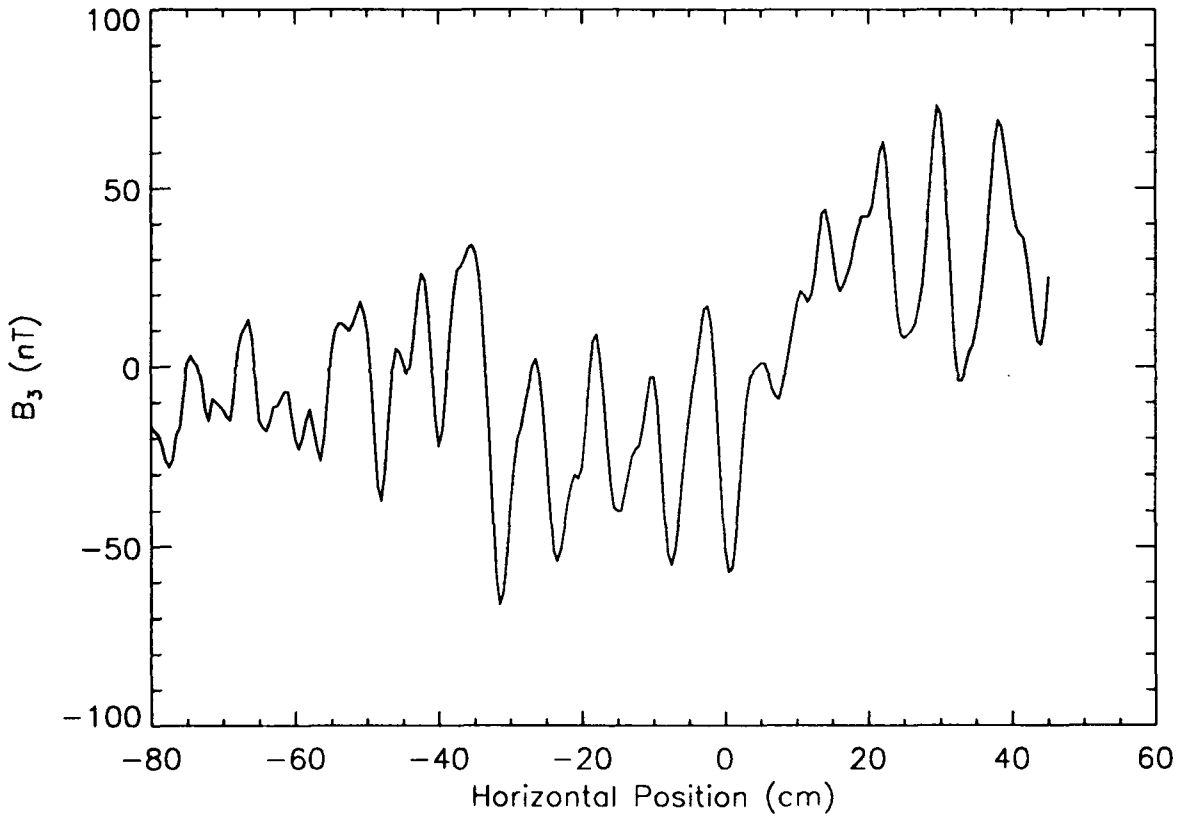

Figure 3.3

Improved DRES rebar detector motion noise. Sensor unit is moving in an east-west direction against a measurement guide to minimize north-south tipping on a smooth measurement table (see Fig. 3.6). Sensor velocity is between 40 and 60 cm/sec. The method and equipment are described in Section 3.2.

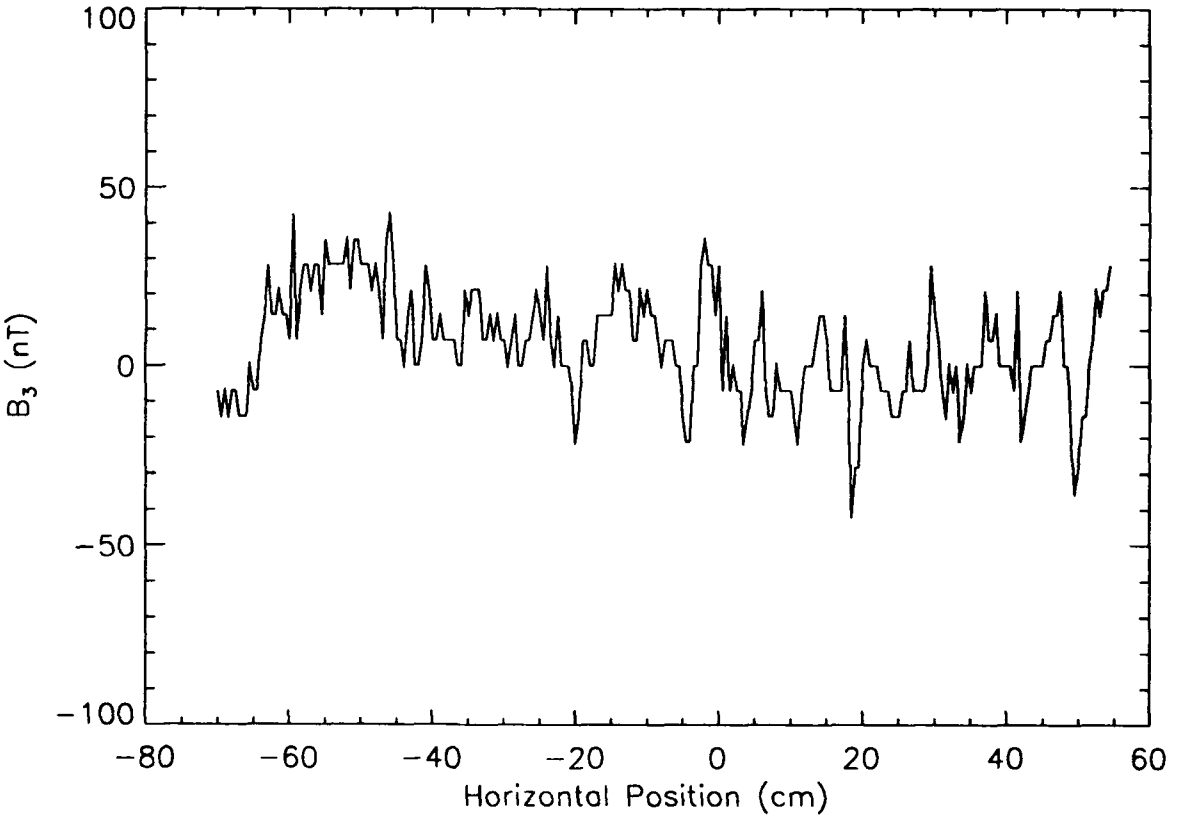

Figure 3.4

Improved DRES rebar detector motion noise after final modifications. Sensor unit is moving in an east-west direction against a measurement guide to minimize north-south tipping on a smooth measurement table (see Fig. 3.6). Sensor velocity is between 40 and 60 cm/sec. The method and equipment are described in Section 3.2.

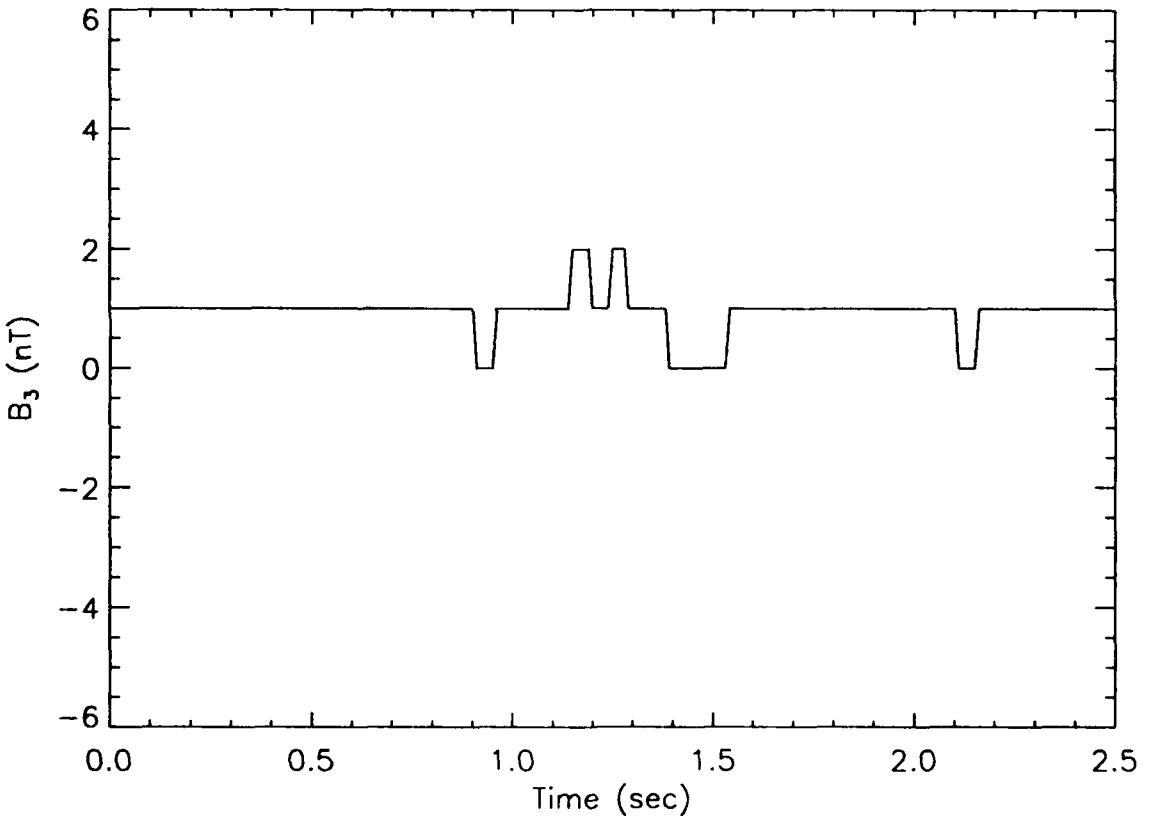

Figure 3.5

Stationary improved DRES rebar detector noise.

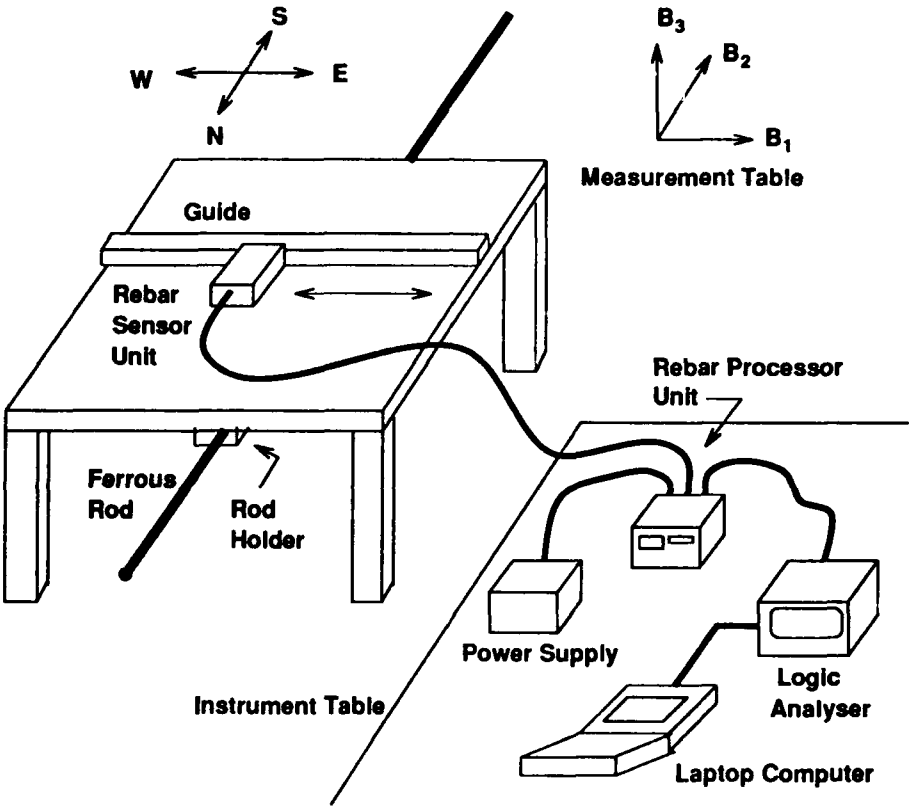

Figure 3.6

Experimental set-up for measurement of magnetic fields of ferrous rods.

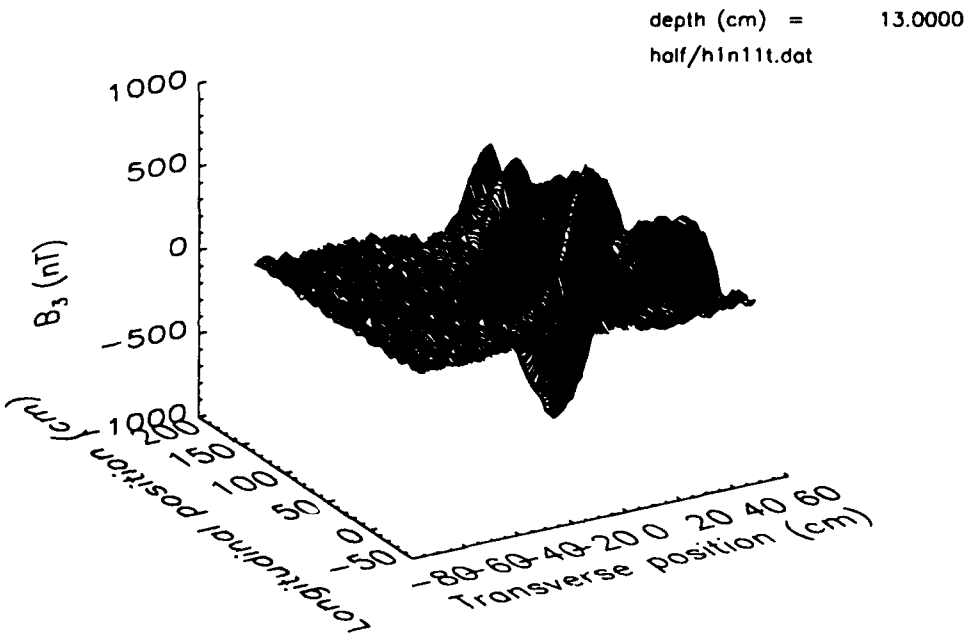

Figure 3.7

Map of the vertical component of the magnetic field in a horizontal plane due to a horizontal 1.27 cm diameter, 143.0 cm long mild steel rod (rod h1). The axis of the rod is 13 cm below the measurement surface and is oriented in a north-south direction.

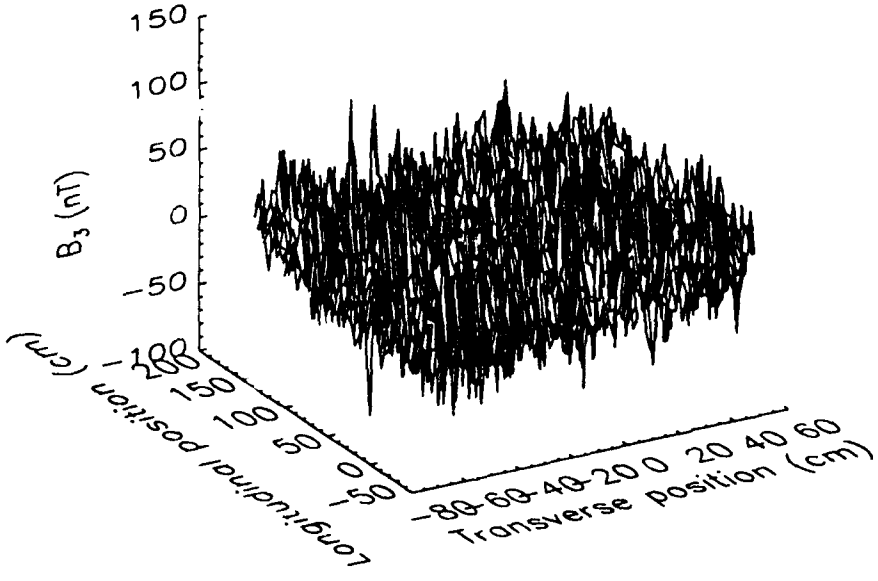

Figure 3.8

Difference between two magnetic maps of a 1.27 cm diameter 143.0 cm long mild steel rod at a depth of 13.0 cm.

4. Experimental Results

4.1 General Observations

The method of Chapter 3 was used to obtain magnetic maps of a number of horizontal mild steel rods. The rod labels and dimensions are given in Table I. The letters "h", "1q" and "3q" in the label refer to "half", "one quarter" and "three quarters", which are the respective diameters in inches. The number following the letter is an index to length, such that rods of the same index have equal lengths (±2 mm). Most of the rods were roughly 1.5 m in length, which is typical of the length of some reinforcing steel and long enough to make valid the long rod approximation. The two ~ 3/4 m length rods were used to determine effects due to the length of the rod by comparison with rods roughly twice as long.

Label	Diameter (cm ± 1 mm)	Length (cm ± 1 mm)
h1	1.270	143.0
h2	1.270	140.5
h3	1.270	75.0
h4	1.270	74.5
h5	1.270	149.7
1q1	0.635	143.0
1q2	0.635	140.5
1q5	0.635	149.5
3q5	1.905	149.7

Table I

Physical dimensions of rods used in experiments. Rods h3,h4,h5 are cut from the same stock which is different from the stock for h1,h2.

In all the magnetic field maps that follow, the rod axis lies directly under the 0 transverse position ($x_1 = 0$) and one end of the rod lies directly under the 0 longitudinal position

(x_2=0). Figs. 4.1, 4.2 and 4.3 illustrate magnetic field vertical component maps for rod h2 at 8, 13 and 18 cm depths respectively. (The narrow spikes on Fig. 4.1 are artifacts due to an instability encountered in the magnetometer signal conditioning chain when the 100 nT/count gain setting was used.) The maximum magnetic field is seen to decrease with increasing depth, while the width of the peaks increase. The general shape of the field remains the same as the depth varies

Although the general field shapes differ from rod to rod, similar trends with depth occur (Figs. 4.4, 4.5 and 4.6). The variation in shape of the magnetic maps is not due solely to the dimensions of the rods. Figs. 3.7 and 4.2 are magnetic field vertical component maps of rods h1 and h2 at a depth of 13 cm. These rods are identical in diameter, since they come from the same type of bar stock (but not the same rod itself) and are nearly identical in length. The maps have roughly the same peak values, but the shapes of the maps are quite different. This effect is seen in other rods of similar dimensions and at different depths as well. This strongly implies that there is a significant component of remnant magnetization present which is different for each individual rod.

Fig. 4.7 is a magnetic map of rod h1 oriented south-north at a depth of 13 cm. Comparing the magnetic map with that of the same rod at the same depth but oriented north-south (i.e., rotated 180° about a vertical axis) (Fig. 3.7), it is clear that the two maps are substantially different in general shape such as peak placement, number of peaks, shape of peaks and peak heights. The maximum and minimum field values of Fig. 4.7 are about 50% larger in absolute magnitude than those of Fig. 3.7. (Note that the largest positive and negative peaks of Fig. 4.7 exhibit some saturation.) The same effect is noted in comparing the magnetic maps for rod h2 both in the north-south and south-north orientations (Figs. 4.2 and 4.8 respectively). This confirms the presence of a remnant component of the magnetization, since if remnant magnetization were not present, axial and fore-aft symmetry dictate that the magnetic maps for the north-south and south-north orientations should be the same. The remnant magnetization adds to the induced magnetization in one orientation and subtracts from it in the other orientation. A more dramatic example of remnant magnetization is exhibited by rod h5 (Figs. 4.9 and 4.10). In the second Figure, the rod has been rotated 180° about a vertical axis, but the map is now viewed from the other end of the rod. That is, the same end of the rod faces toward the reader in both plots. The magnetic field maps appear very similar in shape and magnitude, showing that the magnetic field has rotated through the same angle as the rod. Since the magnetic field is fixed with respect to a coordinate system attached to the rod, so must be the magnetization. Remnant magnetization has this property, whereas because of symmetry, induced magnetization would not change when the rod was rotated 180° in a horizontal plane. Thus, this suggests that the remnant magnetization is much greater than the induced magnetization. This hypothesis is further strengthened by the much larger maximum field values observed for rod h5 as compared to rods h1 and h2.

Fig. 4.11 shows the magnetic field map of rod h3 which is the same diameter as h1 and h2 but half the length. Comparing with (Figs. 3.7 and 4.2), obtained at the same depth, it is seen that the shape of the map is not simply related to the rod length. However, the longitudinal extent of the map (e.g. the longitudinal spacing between the furthest separated

peaks) does increase as length increases. This clue will be exploited later to estimate rod length. Similar trends are seen for rod h4 which is roughly the same length as h3.

4.2 Comparison With Theory

4.2.1 Infinitely Long Cylinder

Fig. 4.12 shows magnetic scans of the vertical component of the magnetic field in a horizontal plane 8, 13 and 18 cm above a horizontal 1.27 cm diameter, infinitely long ferrous rod oriented north-south. Each scan line is in a horizontal plane in an east-west direction. The magnetic field was calculated using the equations of Section 2.2. Fig. 4.13 shows magnetic scans of the vertical component of the magnetic field in a horizontal plane 13 cm above horizontal infinitely long ferrous rods oriented north-south. The scans correspond to rods of diameter 0.635, 1.27 and 1.905 cm.

Comparison with the previous measured magnetic maps shows at once that the model does not agree with the experimental data. The peak measured fields are significantly larger in magnitude, both negative and positive, than those of the model. In retrospect, the lack of agreement is not surprising. The infinite length approximation must break down near the ends of the rod. Since magnetic flux lines must concentrate at the ends, the measured fields at the rod ends should be much larger than those of the model. One might think, however, that magnetic scans near the center of the rod length would be similar to the scans of the model. Closer scrutiny of the magnetic field maps near the center, however, reveals that the magnetic scans vary dramatically over a small longitudinal distance and even more dramatically from rod to rod. Some of these central scans look roughly like those of the model, while others do not. This can be explained by the previously observed presence of a significant amount of remnant magnetization which varies substantially from rod to rod. The infinite cylinder assumes that there is no remnant magnetization.

4.2.2 Prolate Spheroid

To illustrate the horizontal, long prolate spheroid model of Section 2.3 with the constant diameter approximation, the modelled map of the vertical component of the magnetic field in a horizontal plane 13 cm above a horizontal north-south oriented rod equivalent to rod h1 is shown in Fig. 4.14. It is immediately clear that the modelled and experimental (Fig. 3.7) magnetic fields are not at all similar. The modelled field values are four orders of magnitude larger than the measured field values and the shape of the modelled map is much simpler than that of the experimental map. The longitudinal spacing between the two dominant peaks of the model is much less than the longitudinal spacing between peaks on the central line (0 transverse position) of the experimental map. The modelled map 13 cm above a horizontal north-south oriented rod equivalent to rod h3 is shown in Fig. 4.15. The shape of the model field map for the h3 rod is very similar to that of model for the h1 rod, although

the magnetic field values of the former are roughly a factor of ten smaller than the latter. The model and experimental (Fig. 4.11) field maps for the h3 rod resemble each other more closely than do the maps for the h1 rod, but the model field values for the h3 rod are still about 100 times higher than the experimental values. Similar results occur for other rod dimensions and depths.

The deviation between prolate spheroid model and experimental magnetic field maps is not surprising. First, the magnetization of the cylinder cannot be uniform as required by the spheroid model since the surface of the cylinder cannot be represented by a second order surface [8]. Second, many of the field values are calculated very close to the object. Analysis of the spheroid fields reveals that the maximum octupole field magnitude is about 60 times that of the dipole field for a rod with the dimensions of h1. Also the octupole and dipole fields have an opposite sense; that is, the positive peak of the dipole field roughly coincides with the negative peak of the octupole term. This suggests that the Taylor expansion used in the spheroid model consists of an alternating series and that additional higher order terms are needed to accurately represent the magnetic field.

A more accurate approach to modelling the induced magnetic field would be to use a numerical three dimensional magnetostatic modelling computer code. TDG has the computer code TOSCA (Vector Fields, Aurora, Illinois, USA), based on the scalar potential finite element model of Simkin [14]. It can model both induced and remnant magnetization, if the form of the latter is known. However, the remnant component of magnetization is comparable to the induced magnetization and varies among the experimental rods in an unpredictable manner. Since the form of the remnant magnetization cannot be predicted in advance, neither an analytical nor a numerical modelling method will yield a good estimate of the measured magnetic fields.

Finally, the passband of the magnetometer amplifier filter will add some distortion which will contribute to the deviation between the modelled and experimental magnetic fields. The nominal passband of the filter is 0.1 to 10Hz. The high frequency cutoff is not a significant factor because at the data acquisition speeds used in the experiments, there is not much signal energy above 10 Hz. The most noticable effect is a pronounced undershoot following a large positive peak (e.g., Fig 4.8), due to the AC coupling.

Although the attempts at modelling the magnetic field of a long ferrous rod were unsuccessful, it should be recalled that the primary purpose of these experiments was to devise methods of estimating the rod parameters. In the next Chapter we shall see that most parameters can be estimated even without an accurate model.

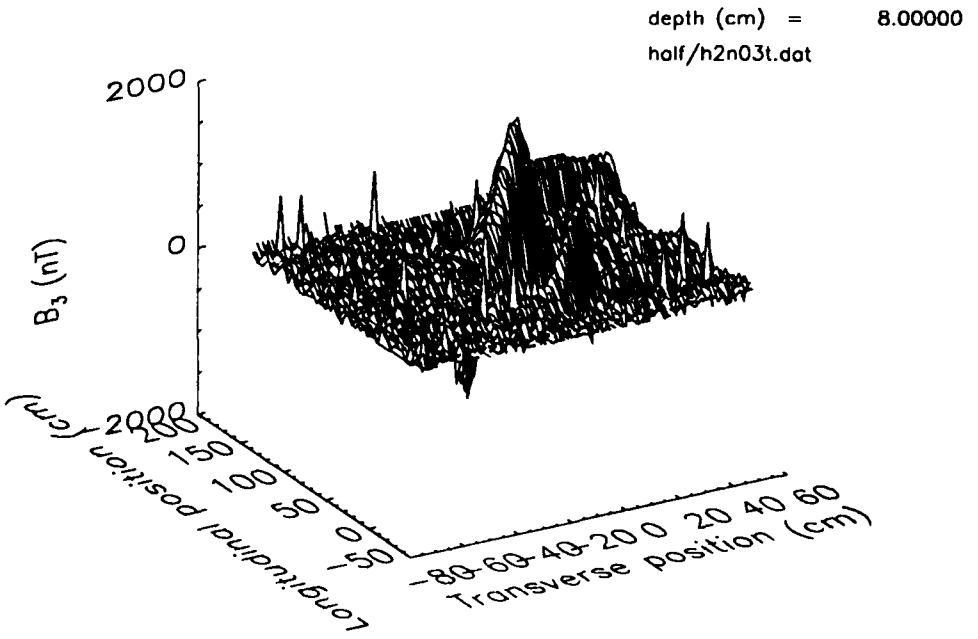

Figure 4.1

Map of the vertical component of the magnetic field in a horizontal plane due to a horizontal 1.27 cm diameter, 140.5 cm long mild steel rod (rod h2). The axis of the rod is 8 cm below the measurement surface and is oriented in a north-south direction.

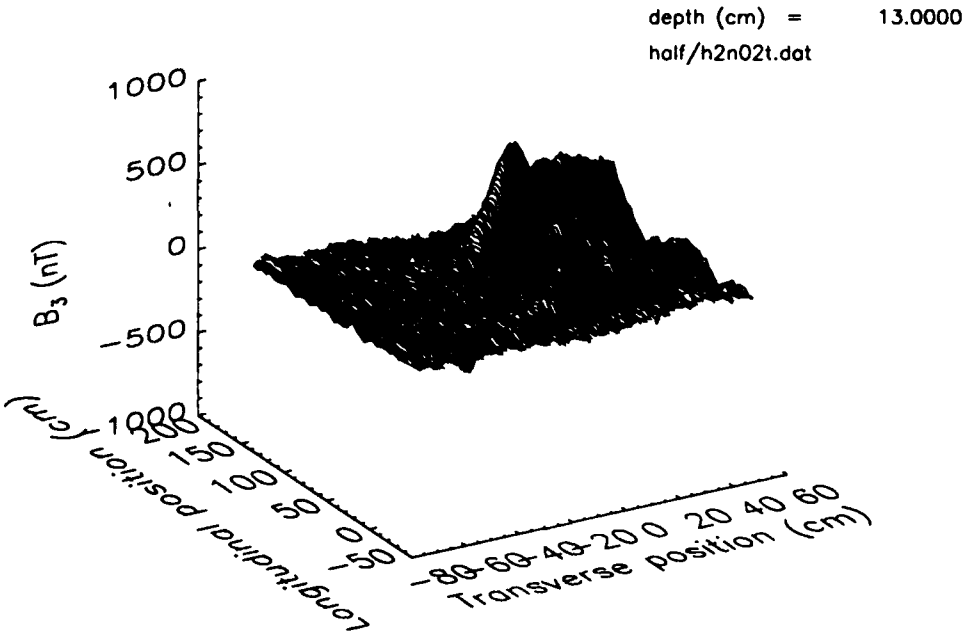

Figure 4.2

Map of the vertical component of the magnetic field in a horizontal plane due to a horizontal 1.27 cm diameter, 140.5 cm long mild steel rod (rod h2). The axis of the rod is 13 cm below the measurement surface and is oriented in a north-south direction.

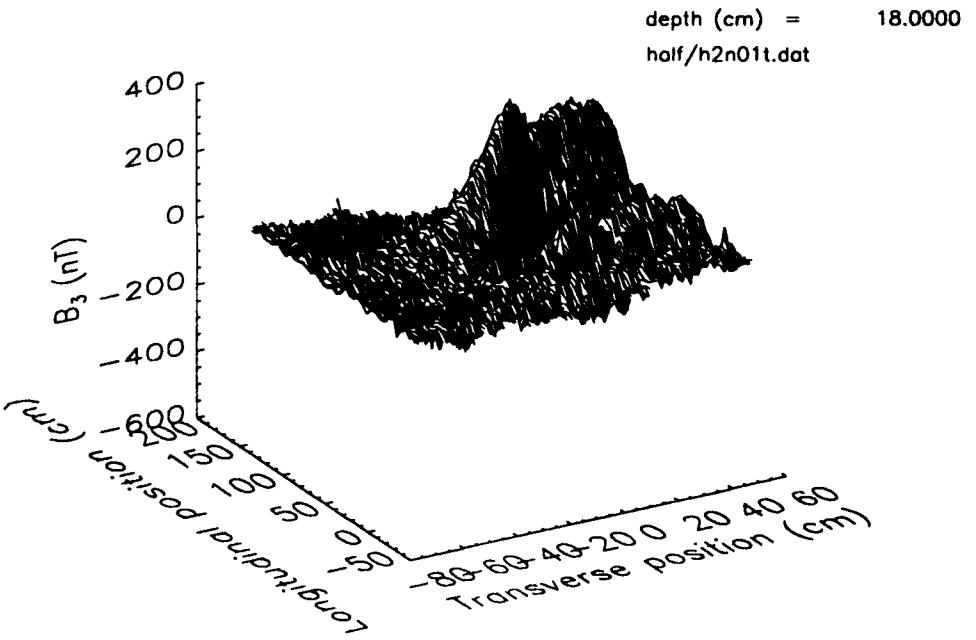

Figure 4.3

Map of the vertical component of the magnetic field in a horizontal plane due to a horizontal 1.27 cm diameter, 140.5 cm long mild steel rod (rod h2). The axis of the rod is 18 cm below the measurement surface and is oriented in a north-south direction.

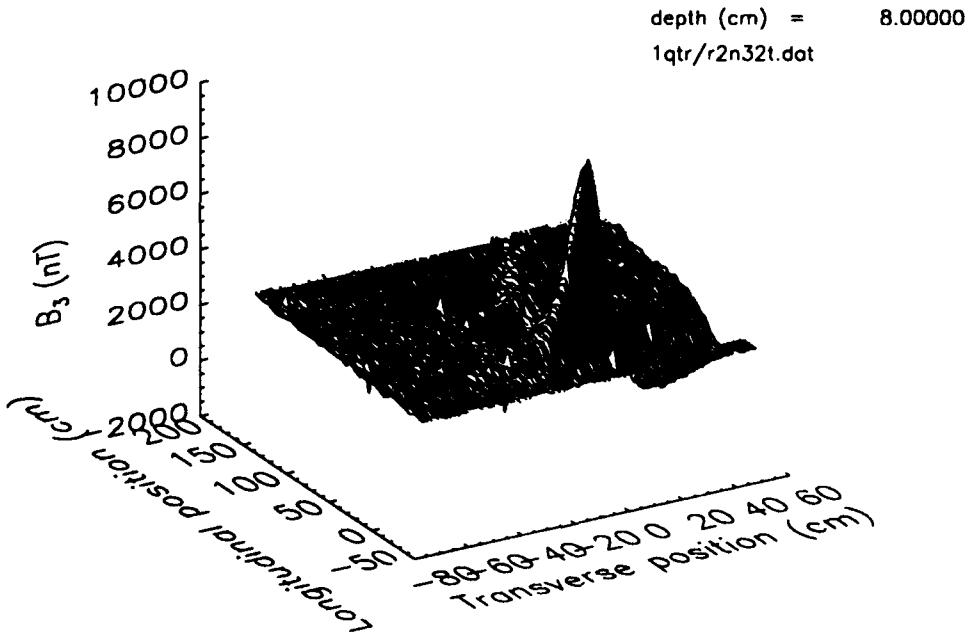

Figure 4.4

Map of the vertical component of the magnetic field in a horizontal plane due to a horizontal 0.635 cm diameter, 140.5 cm long mild steel rod (rod 1q2). The axis of the rod is 8 cm below the measurement surface and is oriented in a north-south direction.

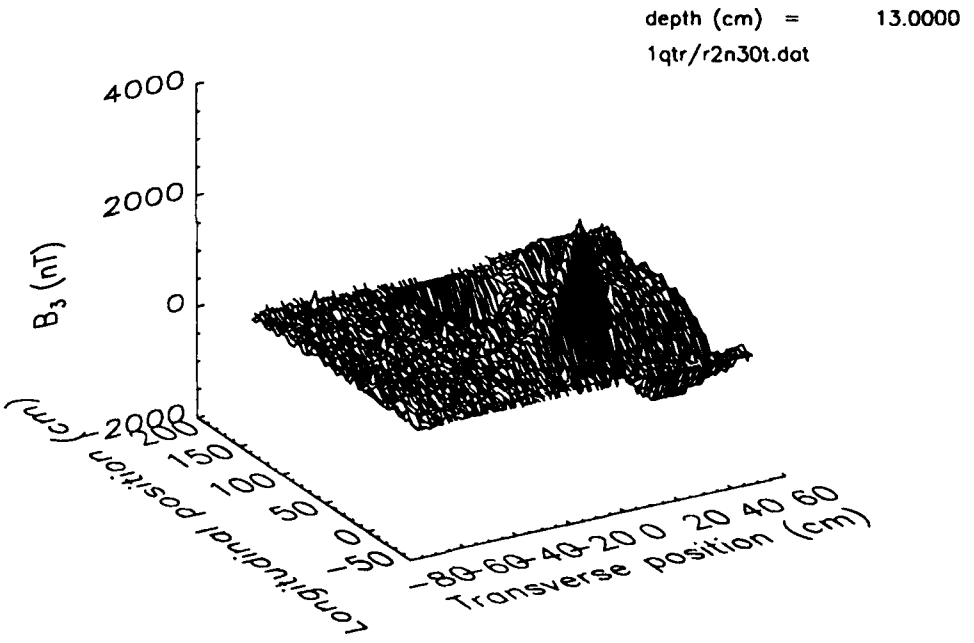

Figure 4.5

Map of the vertical component of the magnetic field in a horizontal plane due to a horizontal 0.635 cm diameter, 140.5 cm long mild steel rod (rod 1q2). The axis of the rod is 13 cm below the measurement surface and is oriented in a north-south direction.

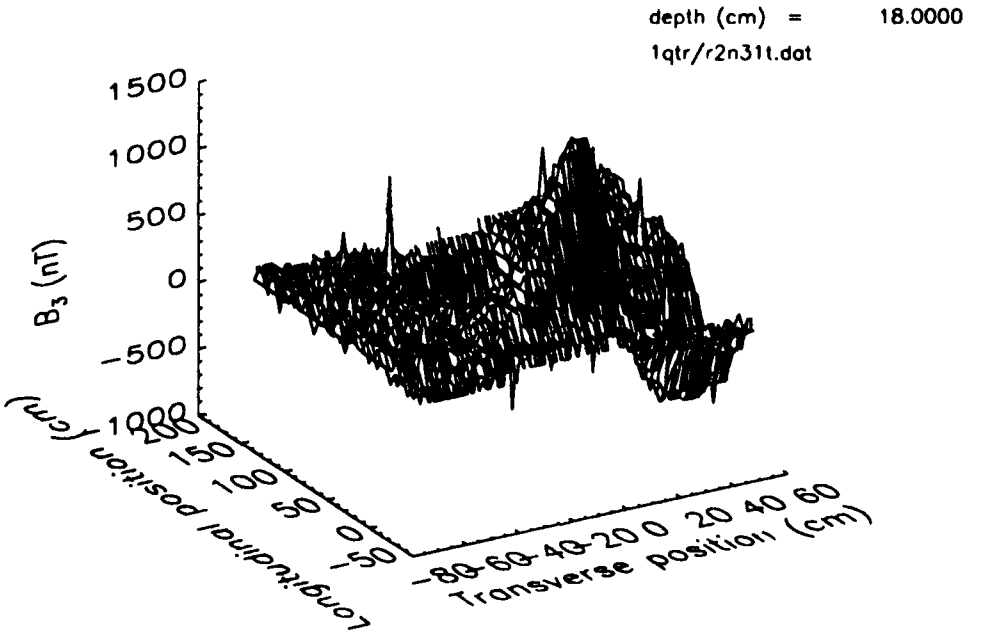

Figure 4.6

Map of the vertical component of the magnetic field in a horizontal plane due to a horizontal 0.635 cm diameter, 140.5 cm long mild steel rod (rod 1q2). The axis of the rod is 18 cm below the measurement surface and is oriented in a north-south direction.

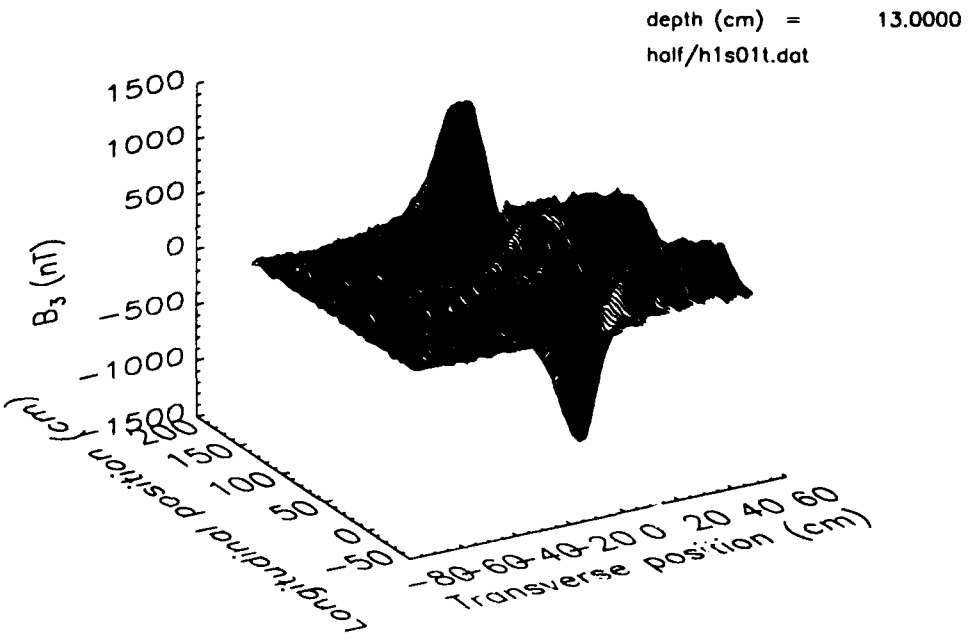

Figure 4.7

Map of the vertical component of the magnetic field in a horizontal plane due to a horizontal 1.27 cm diameter, 143.0 cm long mild steel rod (rod h1). The axis of the rod is 13 cm below the measurement surface. The axis is oriented in a south-north direction; that is, rotated 180° about a vertical axis compared to the rod of Fig. 3.7.

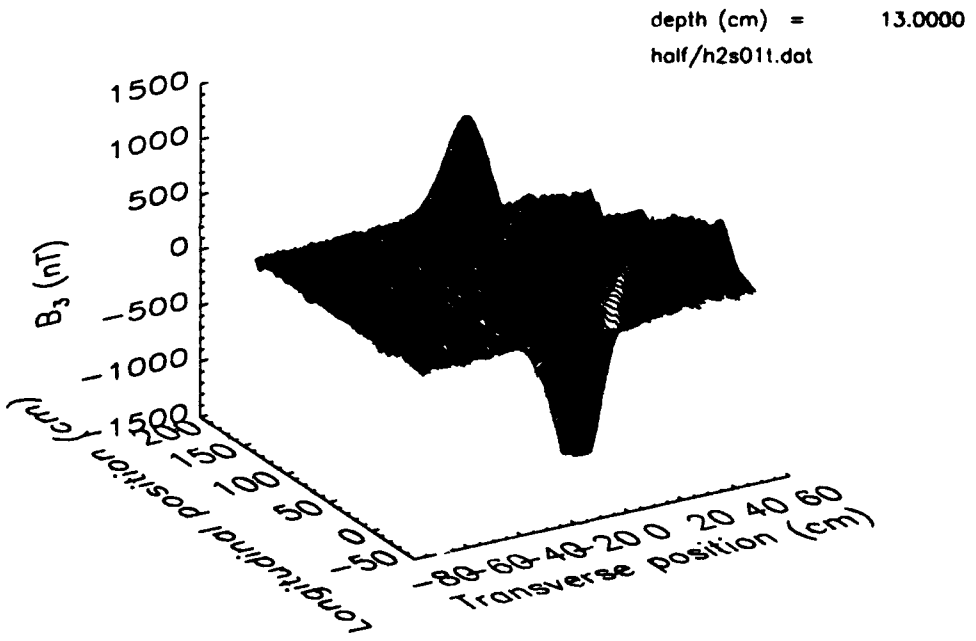

Figure 4.8

Map of the vertical component of the magnetic field in a horizontal plane due to a horizontal 1.27 cm diameter, 140.5 cm long mild steel rod (rod h2). The axis of the rod is 13 cm below the measurement surface. The axis is oriented in a south-north direction; that is, rotated 180° about a vertical axis compared to the rod of Fig. 4.2.

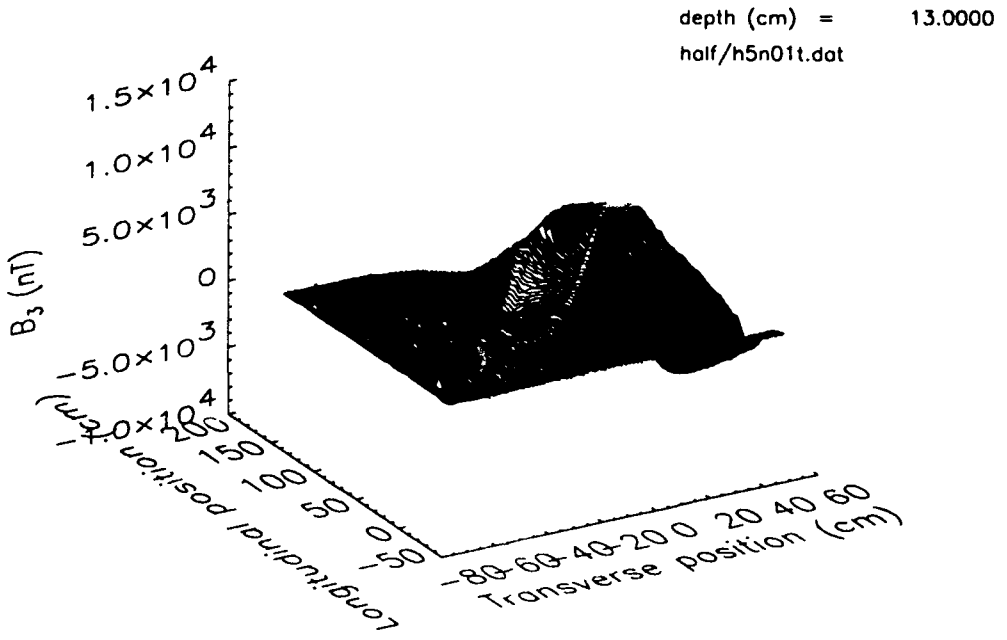

Figure 4.9

Map of the vertical component of the magnetic field in a horizontal plane due to a horizontal 1.27 cm diameter, 149.7 cm long mild steel rod (rod h5). The axis of the rod is 13 cm below the measurement surface. The axis is oriented in a north-south direction.

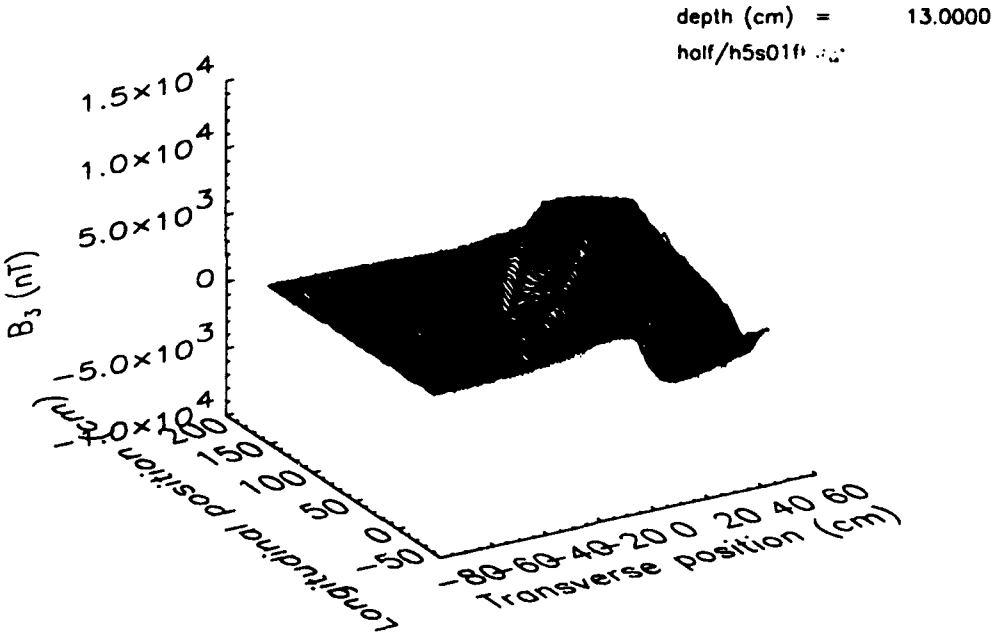

Figure 4.10

Map of the vertical component of the magnetic field in a horizontal plane due to a horizontal 1.27 cm diameter, 149.7 cm long mild steel rod (rod h5). The axis of the rod is 13 cm below the measurement surface. The axis is oriented in a south-north direction; that is, rotated 180° about a vertical axis compared to the rod of Fig. 4.9.

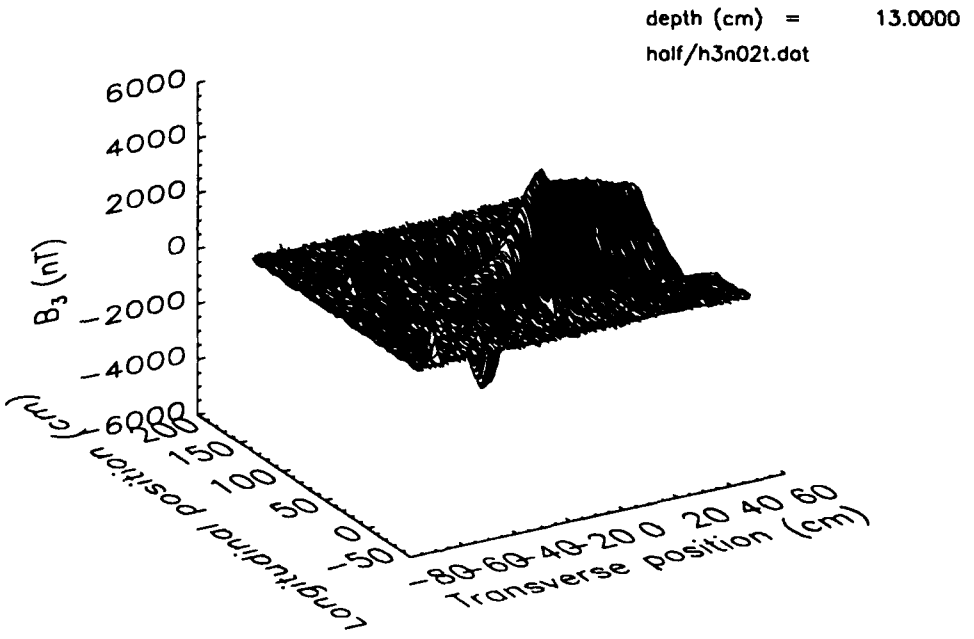

Figure 4.11

Map of the vertical component of the magnetic field in a horizontal plane due to a horizontal 1.27 cm diameter, 75.0 cm long mild steel rod (rod h3). The axis of the rod is 13 cm below the measurement surface. The axis is oriented in a north-south direction. Compare with Figs. 3.7 and 4.2.

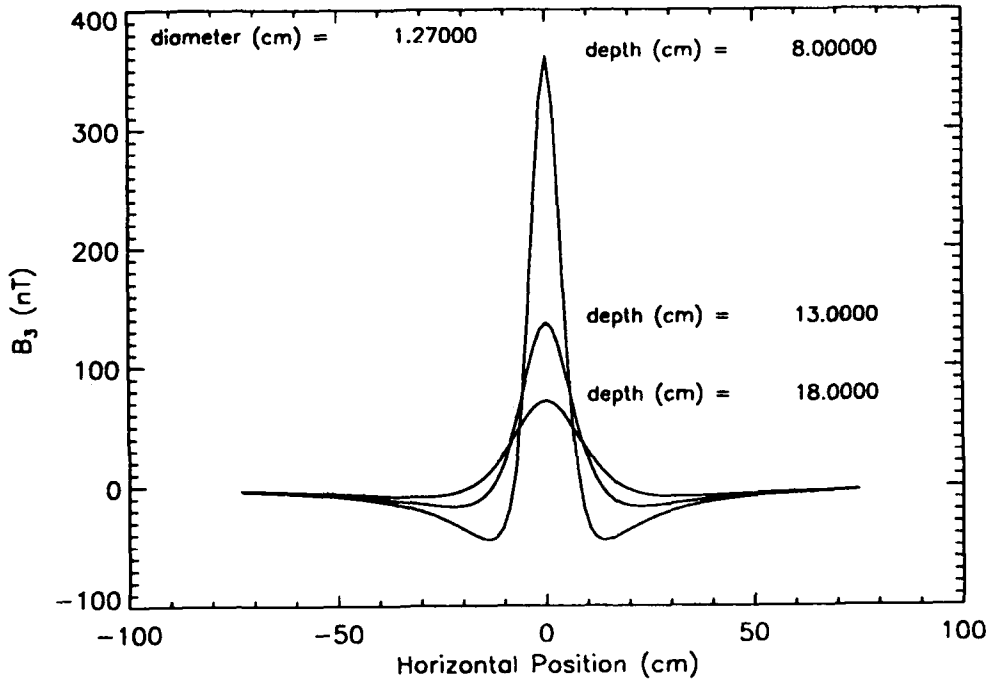

Figure 4.12

Variation of B_3 with position in a horizontal plane along a line orthogonal to the symmetry axis of a horizontal 1.27 cm diameter, infinitely long ferrous rod oriented in a north-south direction. Scans are shown for three different depths.

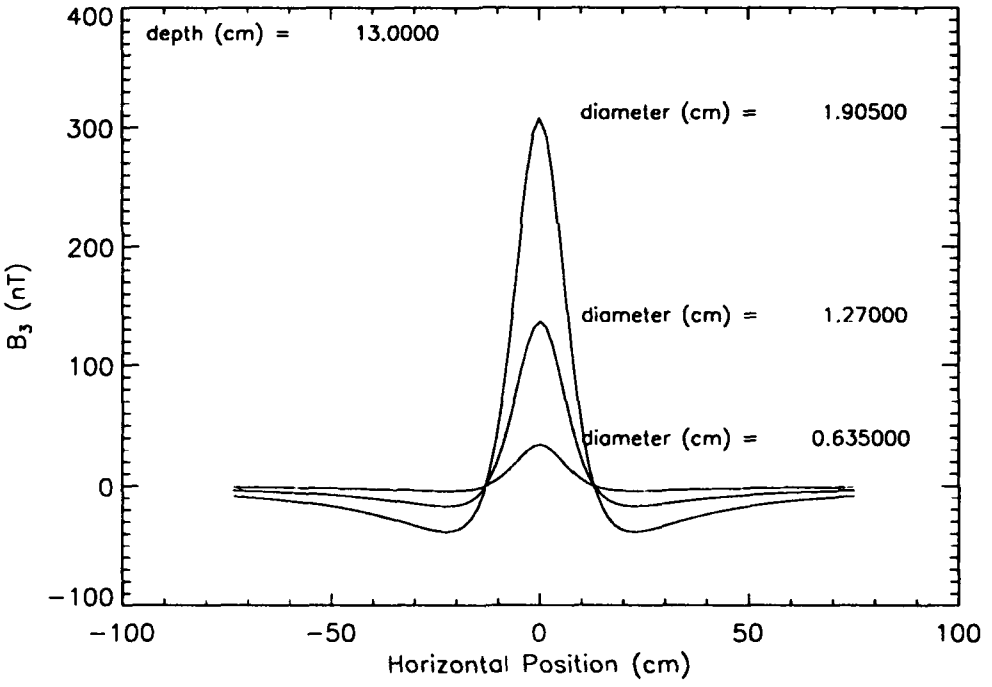

Figure 4.13

Variation of B_3 with position in a horizontal plane along a line orthogonal to the symmetry axis of three horizontal infinitely long ferrous rods of different diameters oriented in a north-south direction. The depth of all three rods is 13 cm.

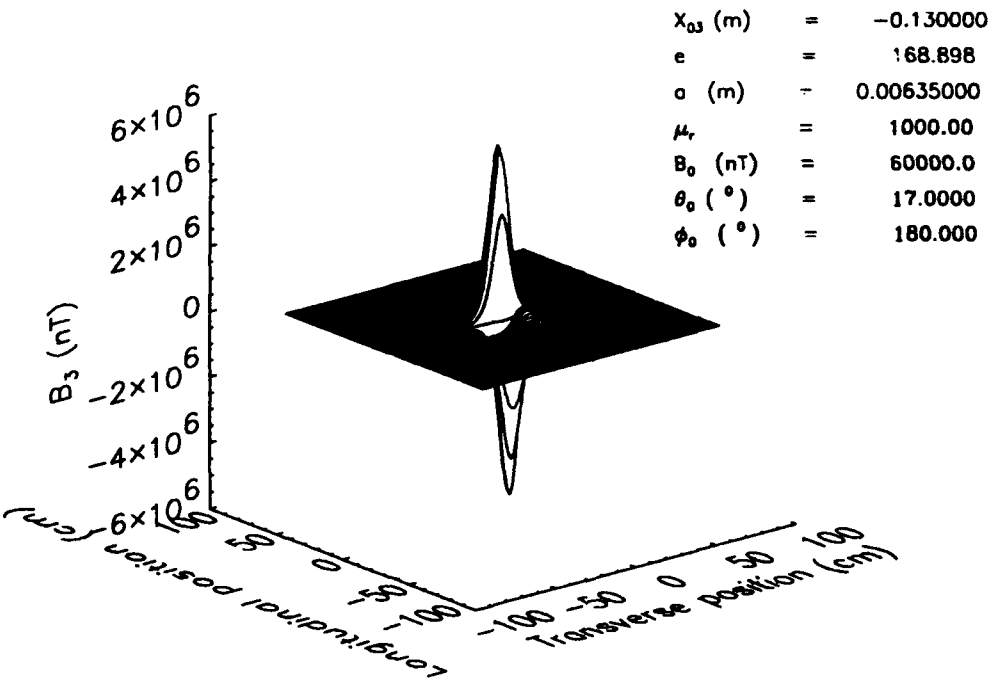

Figure 4.14

Map of the vertical component of the magnetic field in a horizontal plane 13 cm above a prolate spheroid model of a horizontal 1.27 cm diameter, 143.0 cm long ferrous rod (h1). The rod is oriented north-south. Spheroid model parameters are shown on the figure and are defined in Section 2.3.

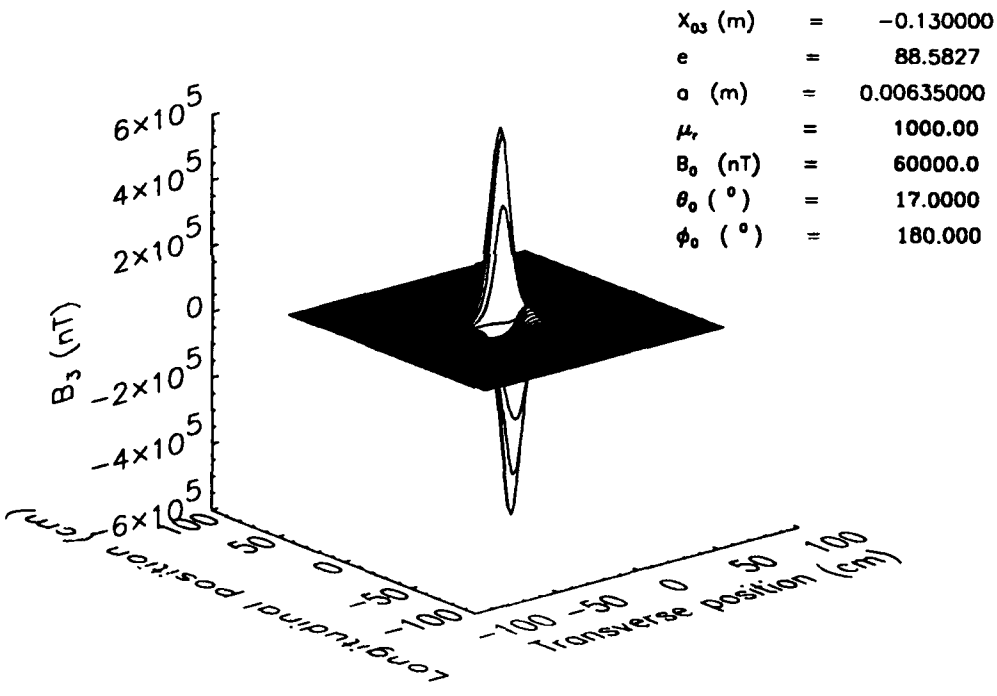

Figure 4.15

Map of the vertical component of the magnetic field in a horizontal plane 13 cm above a prolate spheroid model of a horizontal 1.27 cm diameter, 75.0 cm long ferrous rod (h3). The rod is oriented north-south. Spheroid model parameters are shown on the figure and are defined in Section 2.3.

5. Estimation of Rod Parameters

In this Chapter we investigate simple features of the magnetic field distribution in a horizontal plane which could be used to estimate the parameters of a horizontal rod; i.e., the orientation angle in the horizontal plane, the depth, length and diameter. It must be cautioned that the results to be presented have only been verified for horizontal rods oriented in a north-south direction.

5.1 Estimation of Orientation Angle in the Horizontal Plane

Inspection of any experimental magnetic field map of a single rod revealed that the largest positive and negative peaks lay near the projection of the axis of the rod in the horizontal plane. (Interestingly, even though both the spheroid and the infinite cylinder models did not approximate the experimental data well, the peaks of their magnetic maps also lay along the rod axis.) This suggested a simple way to determine the orientation of a rod in the horizontal plane. Practical implementation was slightly more complicated since scans with small magnetic field values (relative to the absolute maxima of the map) did not always have peaks near the rod axis and some of these scans did not even have clearly defined peaks. Many methods of selecting scans with the larger peaks for peak position estimation were studied. The following method was chosen as being the most accurate and robust.

The scans were ordered on the basis of the largest absolute value for each scan. Each scan was first convolved with a 15 point smoothing filter to provide a preliminary spike rejection. (In the end, results with and without the smoothing filter turned out to be very similar.) The position of the peak and the full width at half maximum (FWHM) were determined for the first n scans. If two scans were tied in maximum field value, both were used. A scan was rejected if the FWHM was greater than 50 cm or less than 2 cm. This *ad hoc* rejection was a simple way to implement spike rejection. The mean and standard deviation of both the position of the peak and the FWHM were calculated from the individual values of these quantities for the n scans. A value of $n = 5$ or 6 was found to minimize the standard deviations in the mean estimates of peak position and FWHM. These results are summarized in Table II.

The mean and standard deviation of the peak position for a given depth were obtained

File Name	Rod Label	Orientation (North or South)	Number of Scans to Estimate Mean (n)	Mean Peak Transverse Position ± Standard Deviation (cm ± cm)	Mean FWHM ± Standard Deviation (cm ± cm)
depth = 8.0 cm					
r1n32t	1q1	N	6	3.0 ± 0.7	14.9 ± 1.0
r2n32t	1q2	N	6	2.3 ± 0.4	13.6 ± 0.6
r5n32t	1q2	N	6	2.4 ± 0.6	13.7 ± 0.6
h1n15t	h1	N	5	1.6 ± 0.6	12.4 ± 2.2
r1n12t	h1	N	6	-1.9 ± 1.0	15.3 ± 1.7
h2n03t	h2	N	6	0.7 ± 0.9	11.1 ± 2.0
depth = 13.0 cm					
r1n30t	1q1	N	6	1.7 ± 0.3	19.7 ± 0.6
r2n30t	1q2	N	6	0.4 ± 1.6	19.4 ± 1.4
r5n30t	1q5	N	6	1.5 ± 1.2	19.4 ± 1.3
h1n14t	h1	N	6	1.4 ± 1.2	19.3 ± 2.9
h1s01t	h1	S	6	1.9 ± 1.0	18.6 ± 0.9
h2n02t	h2	N	6	0.8 ± 1.2	17.6 ± 1.1
h2n04t	h2	N	6	0.3 ± 1.0	17.7 ± 1.1
h2s01t	h2	S	6	-1.5 ± 1.8	18.9 ± 1.6
h3n01t	h3	N	6	0.0 ± 1.0	18.3 ± 0.6
h3n02t	h3	N	6	-1.9 ± 0.9	17.8 ± 0.6
h4n01t	h4	N	6	-0.4 ± 0.5	18.5 ± 0.5
h5n01t	h5	N	6	-0.4 ± 0.5	18.7 ± 0.4
h5s01t	h5	S	6	-0.8 ± 0.4	18.4 ± 0.6
r5n20t	3q5	N	6	3.0 ± 0.3	19.6 ± 1.3
depth = 18.0 cm					
r1n31t	1q1	N	6	0.4 ± 0.7	23.9 ± 0.9
r2n31t	1q2	N	5	-0.7 ± 1.5	23.6 ± 0.9
r5n31t	1q5	N	6	0.7 ± 1.7	26.3 ± 0.6
h1n16t	h1	N	6	0.7 ± 2.7	23.5 ± 2.5
r1n11t	h1	N	6	0.5 ± 1.9	24.4 ± 2.5
h2n01t	h2	N	6	0.3 ± 0.9	24.2 ± 1.6
r2n11t	h2	N	6	-1.4 ± 1.8	23.9 ± 1.3
r5n11t	h5	N	6	0.0 ± 0.8	25.2 ± 0.8
r5n21t	3q5	N	6	0.0 ± 1.5	24.5 ± 1.5

Table II

Estimates of full width at half maximum (FWHM), transverse position of magnetic field maximum and their standard deviations for all rods and depths.

Depth (cm)	Mean Position of Maximum (cm)	Standard Deviation of Position (cm)	Number of Data Points	Reduced χ^2
8	1.90	0.51	6	4.1
13	1.06	0.42	14	7.7
18	0.14	0.16	9	0.2
all	1.17	0.27	29	5.0

Table III

Mean positions of maxima of magnetic field scans versus rod depth. Criteria for choosing which scans to include in the average is explained in the text.

by performing a weighted least squares fit to a constant using the mean peak positions from Table II for all cases corresponding to that depth. The overall mean and standard deviation of the peak position for all depths was also calculated in a similar manner. These results are shown in Table III.

The mean transverse positions of all the maxima and their associated uncertainties are plotted in Fig. 5.1 together with the best fit position to all points (the fit parameters are given in the last row of Table III).

Theoretical and experimental data on spheroids [3] show that for a given ambient field direction, the positions of field maxima in a plane are a function of object depth even when a significant octupole field contribution is present. This is also true for the theory of the infinite cylinder (Equation 2.8). It is suggestive then to examine whether such a depth dependence exists for the experimental rod data. To study the variation in position of the maxima with depth, we used the mean estimates which were calculated for each depth (Table III). A weighted least squares fit was then performed on these data points both to a constant and to a straight line function of depth. The best fit to a constant was given by

$$x_{max} = (0.39 \pm 0.38) \tag{5.1}$$

where x_{max} is the position (in cm relative to the point directly above the rod axis) of the maximum field value in the transverse direction. The reduced χ^2 was 6.9 for 2 degrees of freedom. Uncertainties in coefficients were derived from the theory of linear least squares fitting [15]. The best fit to a straight line with depth was given by

$$x_{max} = (3.35 \pm 0.07) + (-0.179 \pm 0.004)z \tag{5.2}$$

where z is the depth (cm). The reduced χ^2 was 0.007 for 1 degree of freedom. The straight line fit is shown in Fig. 5.2.

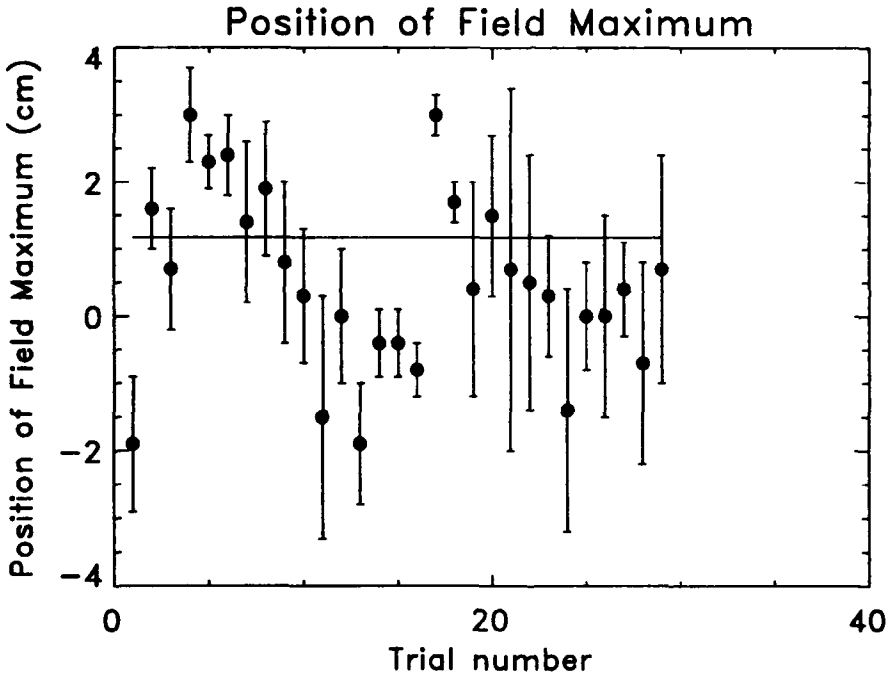

Figure 5.1

Positions of maxima of magnetic field scans for all rod lengths and depths. Straight line is the least squares fit to a constant. Error bars represent one standard deviation of the position estimate.

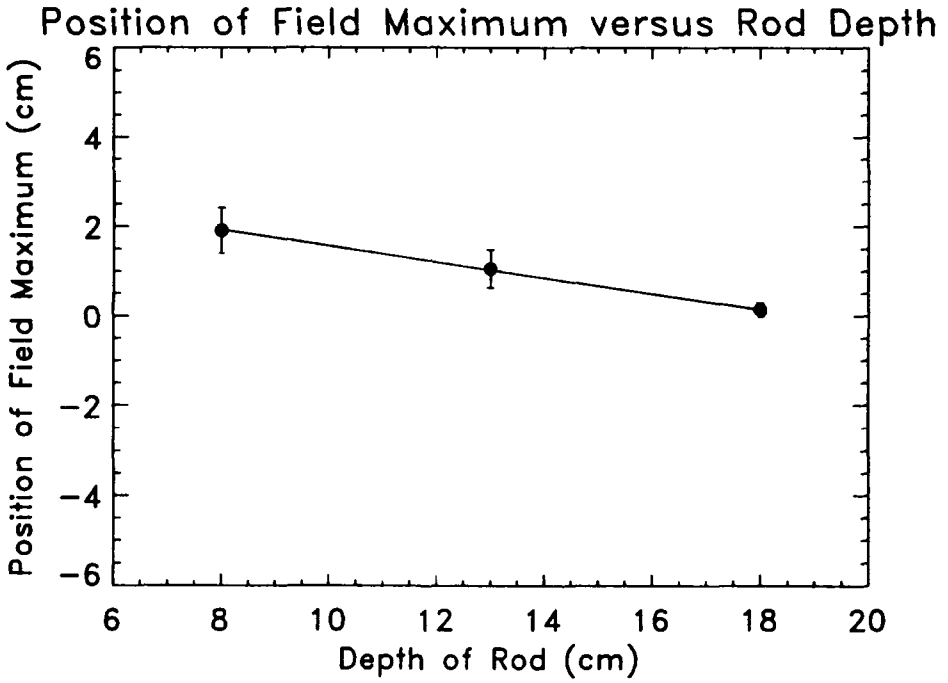

Figure 5.2

Mean positions of maxima of magnetic field scans versus rod depth. Criteria for choosing which scans to include in the average is explained in the text. Error bars represent one standard deviation of the mean estimate. Solid line is the best fit to a straight line.

Depth (cm)	Mean Full Width at Half Maximum (cm)	Standard Deviation of FWHM (cm)	Number of Data Points	Reduced χ^2
8	13.8	0.3	6	0.9
13	18.6	0.2	14	0.7
18	24.9	0.4	9	1.3

Table IV

Mean full width at half maximum of magnetic field scans versus rod depth. Criteria for choosing which scans to include in the average is explained in the text.

It is quite clear that, to within experimental errors, there is a straight line variation of peak position with depth and that the straight line fit is superior to the fit to a constant. The depth variation is not strong, however. Also, it must be remembered that the span of depths over which the fit was performed is quite limited and extrapolation to estimate the variation outside this range is prone to large errors.

5.2 Estimation of Rod Depth

Evidence suggests that it may be possible to determine an empirical relation between the FWHM of a magnetic scan and the depth for a horizontal ferrous rod. The simple theory of the infinite horizontal rod shows that the depth of a rod is equal to the FWHM times a proportionality constant (Equation 2.6). The theory of the spheroid yields a more complicated function relating depth and FWHM [3], but it is still monotonic. For a number of other objects, the width of the field in a plane also varies monotonically with depth and if the orientation of a dipole is fixed, the width of the field in a plane is a monotonic function of depth [2]. To try to find a relationship between FWHM and depth, the weighted average of the FWHM and its corresponding standard deviation were determined for a given depth using the mean FWHM and standard deviations for all rods at that depth from Table II. The results are given in Table IV.

The FWHM clearly varies with depth. Since only three data points are available, a quadratic is the highest order polynomial function of depth to which the data can be fitted. Although a quadratic function does fit the data slightly better than a straight line function, one cannot estimate the quadratic fitting error because it is an exact fit. The fit to a straight line is shown in Fig. 5.3. The data appears to be reasonably well modelled by the straight line as is further evidenced by the reduced χ^2 of 5.5 for 1 degree of freedom. The equation

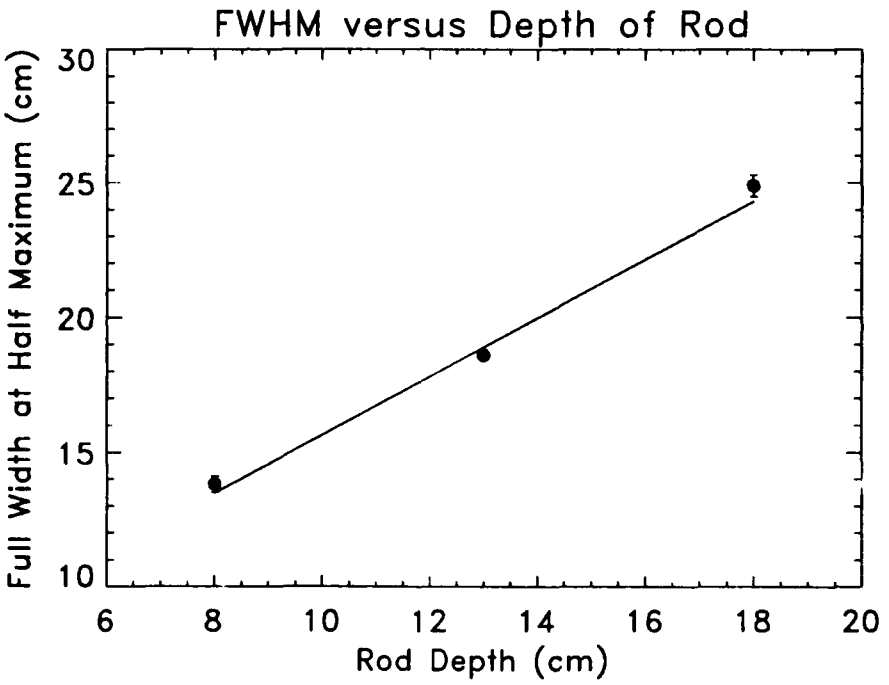

Figure 5.3

Mean full width at half maximum of magnetic field scans versus rod depth. Criteria for choosing which scans to include in the average is explained in the text. Error bars represent one standard deviation of the mean estimate. Solid line is the best fit to a straight line.

which expresses the FWHM as a function of depth is

$$x_{1/2} = (1.08 \pm 0.11)z + (4.80 \pm 1.47) \tag{5.3}$$

where $x_{1/2}$ is the full width at half maximum and z is the rod depth, both in cm.

5.3 Estimation of Rod Length

The last parameters needed to localize the rod are the positions of the ends of the rod. Two methods to estimate the end point positions were investigated. The first estimated the end point to be at the x_2 or longitudinal position for which the field in the measurement plane along the rod axis ($x_1 = 0$) had ultimately decreased to a fraction times the greater of the absolute value of the largest field maximum or minimum. Fractions of 0.1, 0.25 and 0.5 were tried, with the first two giving the best results. Even so, the variation of estimates of rod length for maps of the same rod and depth were between 15 and 20 cm.

The second method assumed the end point positions to coincide with the furthest longitudinally displaced significant central peak. A significant central peak is a field maximum or minimum which is above the rod axis ($x_1 = 0$) and whose absolute value is greater than 25% of the absolute value of the largest maximum or minimum. The results of the second method are shown in Tables V and VI.

The uncertainty in estimating each peak position is governed by the effective noise near the peak and the shape of the peak. It can be estimated by repeatedly measuring the position of a particular peak and is found to be approximately 3 to 4 cm. The rod end position estimates may exhibit a slight depth variation which differs from rod to rod, but the trend is only marginally above the uncertainty in estimating peak positions. The chief factor which governs the error in rod end position estimates is the particular rod being measured. The average estimate of the southern end position for rod h1 (4.1 ± 1.5 cm) is significantly closer to the true position than is the average estimate for the other rods (11.2 ± 3.6 cm). Qualitatively, this must be due to a difference in the distribution of remnant magnetization in h1 compared to the other rods, but there is as yet no quantitative explanation. Interestingly, with the exception of rod h1, the average position estimate for the southern end is much farther from the true position than the average position estimate for the northern end (-0.6 ± 3.4 cm), even though the standard deviations are similar. It was at first thought that this was due to the rod axis lying in the vertical plane of the earth's magnetic field vector. This breaks any fore-aft symmetry, so one should not expect the most southern magnetic field peak to be in the same position relative to its corresponding rod end as the most northern peak. However, because the remnant magnetization is attached to a body-fixed coordinate system, there should then be a significant difference in rod end position estimates when a rod is rotated 180° about a vertical axis (i.e., oriented north-south versus south-north). (For example, in the extreme case of negligible induced magnetization, the amount by which an end position is overestimated in one orientation should be the same amount by which it is underestimated in the other orientation.) This is clearly not observed

File Name	Orientation (North or South)	Depth (cm)	South End Position Estimate (cm)	North End Position Estimate (cm)	Rod Length Estimate (cm)	Error in Length Estimate (cm)
Rod h1 (length = 143.0 cm)						
h1n15t	N	8.0	3	1	141	-2
r1n12t	N	8.0	6	1	137	-6
h1n11t	N	13.0	4	2	141	-2
h1n12t	N	13.0	4	1	140	-3
h1n13t	N	13.0	4	1	140	-3
h1n14t	N	13.0	4	2	141	-2
h1s01t	S	13.0	7	4	140	-3
h1n16t	N	18.0	2	4	145	2
r1n11t	N	18.0	3	5	145	2
all			4.1 ± 1.5	2.3 ± 1.6	141.1	-1.9 ± 2.5
Rod h2 (length = 140.5 cm)						
h2n03t	N	8.0	14	1	128	-12
h2n02t	N	13.0	11	-1	128	-12
h2n04t	N	13.0	12	-1	128	-12
h2s01t	S	13.0	12	1	129	-11
h2n01t	N	18.0	11	1	130	-10
r2n11t	N	18.0	14	4	130	-10
all			12.3 ± 1.4	0.8 ± 1.8	129.3	-11.2 ± 1.0
Rod h3 (length = 75.0 cm)						
h3n01t	N	13.0	9	-1	65	-10
h3n02t	N	13.0	8	-3	64	-11
all			8.5 ± 0.7	-2.0 ± 1.4	64.5	-10.5 ± 0.7
Rod h4 (length = 74.5 cm)						
h4n01t	N	13.0	10	-3	63	-12
Rod h5 (length = 149.7 cm)						
h5n01t	N	13.0	9	-3	137	-13
h5s01t	S	13.0	7	-5	137	-13
r5n11t	N	18.0	10	-5	135	-15
all			8.7 ± 1.5	-4.3 ± 1.2	136.0	-13.7 ± 1.2

Table V

Estimates, derived from magnetic field maps, of rod end positions (relative to true end positions), rod length and error in rod length for 1.27 cm diameter horizontal rods.

File Name	Orientation (North or South)	Depth (cm)	South End Position Estimate (cm)	North End Position Estimate (cm)	Rod Length Estimate (cm)	Error in Length Estimate (cm)
Rod 1q1 (diameter = 0.635 cm, length = 143.0 cm)						
r1n32t	N	8.0	12	-2	129	-14
r1n30t	N	13.0	9	1	135	-8
r1n31t	N	18.0	9	5	139	-4
all			10.0 ± 1.7	1.3 ± 3.5	134.3	-8.7 ± 5.0
Rod 1q2 (diameter = 0.635 cm, length = 140.5 cm)						
r2n32t	N	8.0	9	-4	128	-12
r2n30t	N	13.0	9	-5	126	-14
r2n31t	N	18.0	12	-6	122	-18
all			10.0 ± 1.7	-5.0 ± 1.0	125.8	-14.7 ± 3.1
Rod 1q5 (diameter = 0.635 cm, length = 149.5 cm)						
r5n32t	N	8.0	9	-2	139	-11
r5n30t	N	13.0	10	-5	135	-15
r5n31t	N	18.0	11	-8	130	-20
all			10.0 ± 1.0	-5.0 ± 3.0	134.2	-15.3 ± 4.5
Rod 3q5 (diameter = 1.905 cm, length = 149.7 cm)						
r5n20t	N	13.0	17	-1	131	-19
r5n21t	N	18.0	24	3	128	-22
all			20.5 ± 4.9	1.0 ± 2.8	129.2	-20.5 ± 2.1

Table VI

Estimates, derived from magnetic field maps, of rod end positions (relative to true end positions), rod length and error in rod length for 0.635 cm and 1.905 cm diameter horizontal rods.

in Tables V and VI. Hence, there is presently no satisfactory explanation for the difference between south and north rod end estimates relative to the true positions. A likely explanation is an as yet unidentified bias in the process of estimating the most southern peak position.

Overall, the average estimate of rod end position relative to the true position was 9.2 ± 4.5 cm for the southern end and -0.6 ± 3.4 cm for the northern end. The average error in estimation of rod length was -9.8 ± 6.2 cm. This can be expressed by the following equations

$$x_s = x_{cms} - (9.2 \pm 4.5) \tag{5.4}$$

$$x_n = x_{cmn} + (0.6 \pm 3.4)$$

$$l = |x_{cmn} - x_{cms} + 9.8| \pm 6.2$$

where x_s, x_n are respectively the longitudinal positions (x_2 direction) in the horizontal plane of the most southern and northern rod ends, x_{cms}, x_{cmn} are respectively the most southern and northern significant central maxima. A significant central maximum is a maximum or minimum of the magnetic field in the measurement plane along the rod axis ($x_1 = 0$) which is greater than 25% of the absolute value of the largest field maximum or minimum in the plane. l is the rod length and all quantities are in cm.

5.4 Estimation of Rod Diameter

The previous three sections showed how one can estimate the location parameters of the horizontal ferrous rod; that is, the orientation in a horizontal plane, the depth and the position in the horizontal plane of the ends of the rod. The one parameter remaining to be known to completely characterize the rod is its diameter.

The simple theory of infinite rod (Equation 2.7) suggests that, for a given ambient field, the rod diameter is directly proportional to the depth of the rod and directly proportional to the field maximum along a scan direction. The diameter of a prolate spheroid cannot be as simply inferred from the value of the field maximum, but for a fixed orientation, depth and length, the diameter will be monotonically related to the field maximum. Thus, it is of interest to investigate the maxima and minima of the magnetic field in the horizontal measurement plane to see if they exhibit a variation with rod diameter, length and depth.

Figs. 5.4 and 5.5 show the variation of the maximum and minimum values of the magnetic field maps as a function of depth. The absolute values of the field maxima or minima decrease with depth for each rod type.

The maxima and minima exhibit no obvious trend with rod length. For example, rods h3 and h4 are of the same length and from the same stock, but have significantly different maxima and minima. Furthermore, the maxima and minima of rods h3 and h4 lie between those of h5, obtained from the same stock as h3 and h4, and h1 and h2, even though h1, h2 and h5 are all roughly twice the length of h3 and h4.

File Name	Orientation (North or South)	Depth (cm)	Min. (nT)	Max. (nT)
Rod h1 (length = 143.0 cm)				
h1n15t	N	8.0	-1400	2600
r1n12t	N	8.0	< -1280	≈ 1180
h1n11t	N	13.0	-740	870
h1n12t	N	13.0	-720	860
h1n13t	N	13.0	-750	870
h1n14t	N	13.0	-700	850
h1s01t	S	13.0	-1170	1170
h1n16t	N	18.0	-450	370
r1n11t	N	18.0	-410	340
Rod h2 (length = 140.5 cm)				
h2n03t	N	8.0	-2000	1800
h2n02t	N	13.0	-840	730
h2n04t	N	13.0	-820	760
h2s01t	S	13.0	< -1280	≈ 1080
h2n01t	N	18.0	-440	400
r2n11t	N	18.0	-380	380
Rod h3 (length = 75.0 cm)				
h3n01t	N	13.0	-5300	4500
h3n02t	N	13.0	-4900	4300
Rod h4 (length = 74.5 cm)				
h4n01t	N	13.0	-7400	8200
Rod h5 (length = 149.7 cm)				
h5n01t		13.0	-7200	10300
h5s01t	S	13.0	-8300	10600
r5n11t	N	18.0	-3800	5300

Table VII

Maxima and minima of magnetic maps of 1.27 cm diameter horizontal rods. Field values prefaced with a $<$ indicate that the signal conditioning circuit had saturated at the value indicated. Field values prefaced with a $\approx$ were near saturation. The signal conditioning circuit may be operating in a nonlinear fashion and hence the value is approximate.

File Name	Orientation (North or South)	Depth (cm)	Min. (nT)	Max. (nT)
Rod 1q1 (diameter = 0.635 cm, length = 143.0 cm)				
r1n32t	N	8.0	< -1280	≈ 1160
r1n30t	N	13.0	-890	710
r1n31t	N	18.0	-420	350
Rod 1q2 (diameter = 0.635 cm, length = 140.5 cm)				
r2n32t	N	8.0	-800	9400
r2n30t	N	13.0	-1200	2600
r2n31t	N	18.0	-900	1500
Rod 1q5 (diameter = 0.635 cm, length = 149.5 cm)				
r5n32t	N	8.0	-1600	6200
r5n30t	N	13.0	-1700	1500
r5n31t	N	18.0	-850	710
Rod 3q5 (diameter = 1.905 cm, length = 149.7 cm)				
r5n20t	N	13.0	-6400	3800
r5n21t	N	18.0	-3300	2300

Table VIII

Maxima and minima of magnetic maps of 0.635 cm and 1.905 cm diameter horizontal rods. Field values prefaced with a $<$ indicate that the signal conditioning circuit had saturated at the value indicated. Field values prefaced with a $\approx$ were near saturation. The signal conditioning circuit may be operating in a nonlinear fashion and hence the value is approximate. Missing depths for various rods correspond to maps with too many saturated values to allow further analysis.

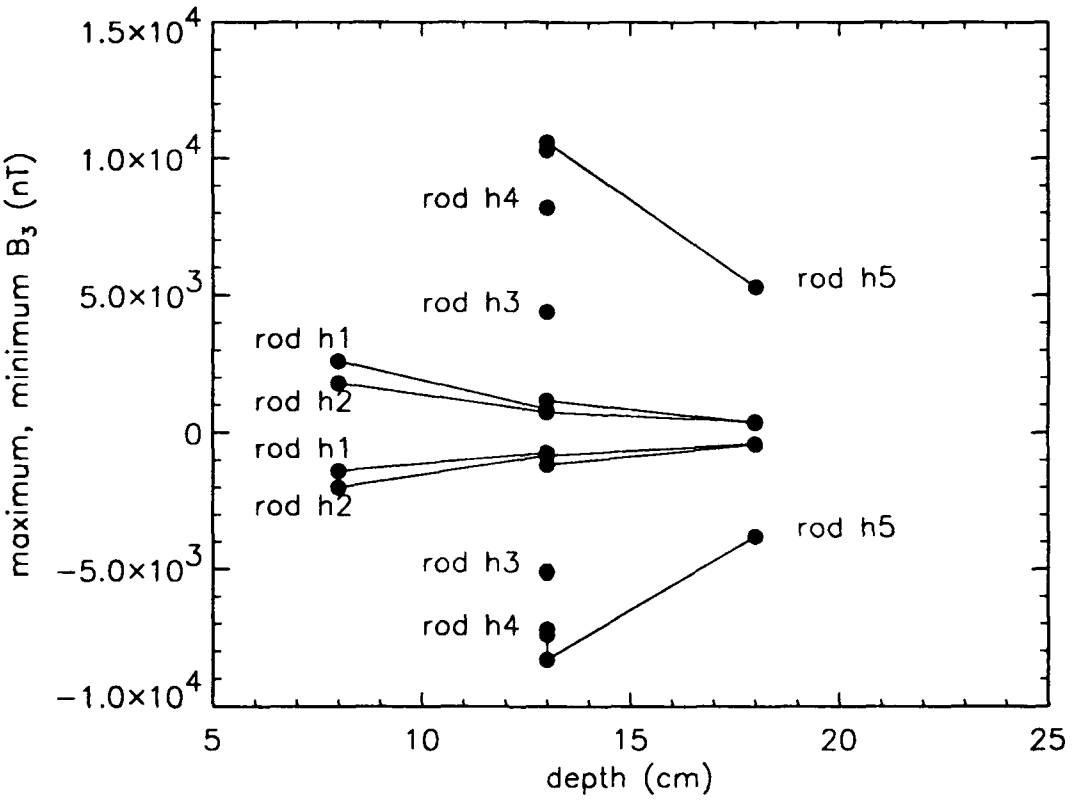

Figure 5.4

Maximum and minimum values of the magnetic field maps versus rod depth for 1.27 cm diameter rods. Maximum values are positive and minimum values are negative in all cases.

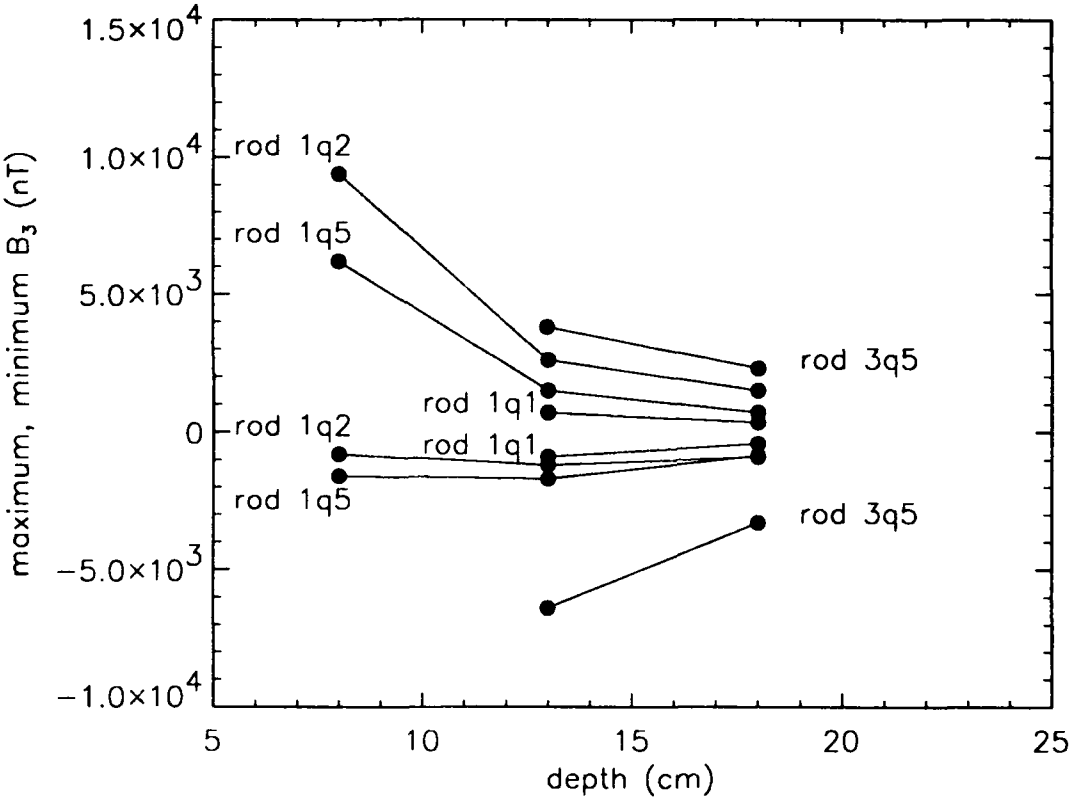

Figure 5.5

Maximum and minimum values of the magnetic field maps versus rod depth for 1.905 and 0.635 cm diameter rods. Maximum values are positive and minimum values are negative in all cases.

To examine the variation of field maxima and minima with rod diameter, we note that depth can be assumed to be known, since it can be estimated independent of rod length or diameter. Figs. 5.6 to 5.8 show the variation of maximum and minimum values of the magnetic field maps versus rod diameter for fixed rod depth. For a wide range of field values at a given depth, the maximum and minimum field are multivalued functions of rod diameter. This is chiefly due to the wide variation in remnant magnetization as discussed earlier and makes estimation of rod diameter from the magnetic field map very difficult.

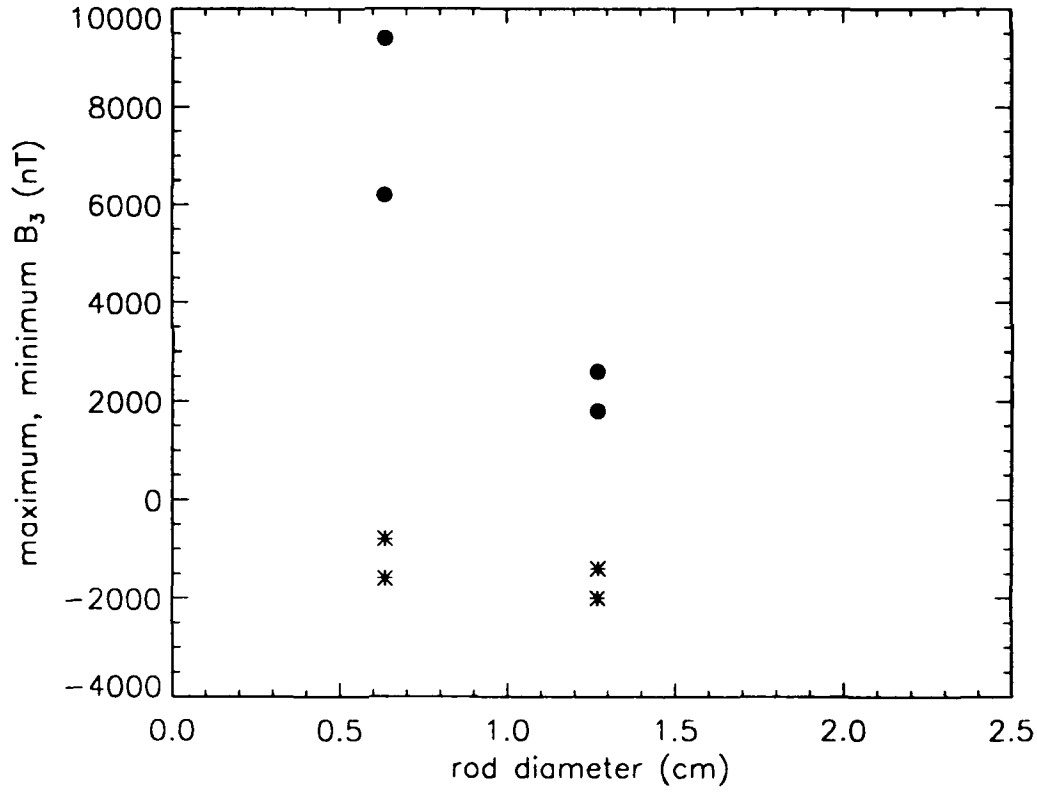

Figure 5.6

Maximum (dots) and minimum (stars) values of the magnetic field maps versus rod diameter for all rods at a depth of 8 cm.

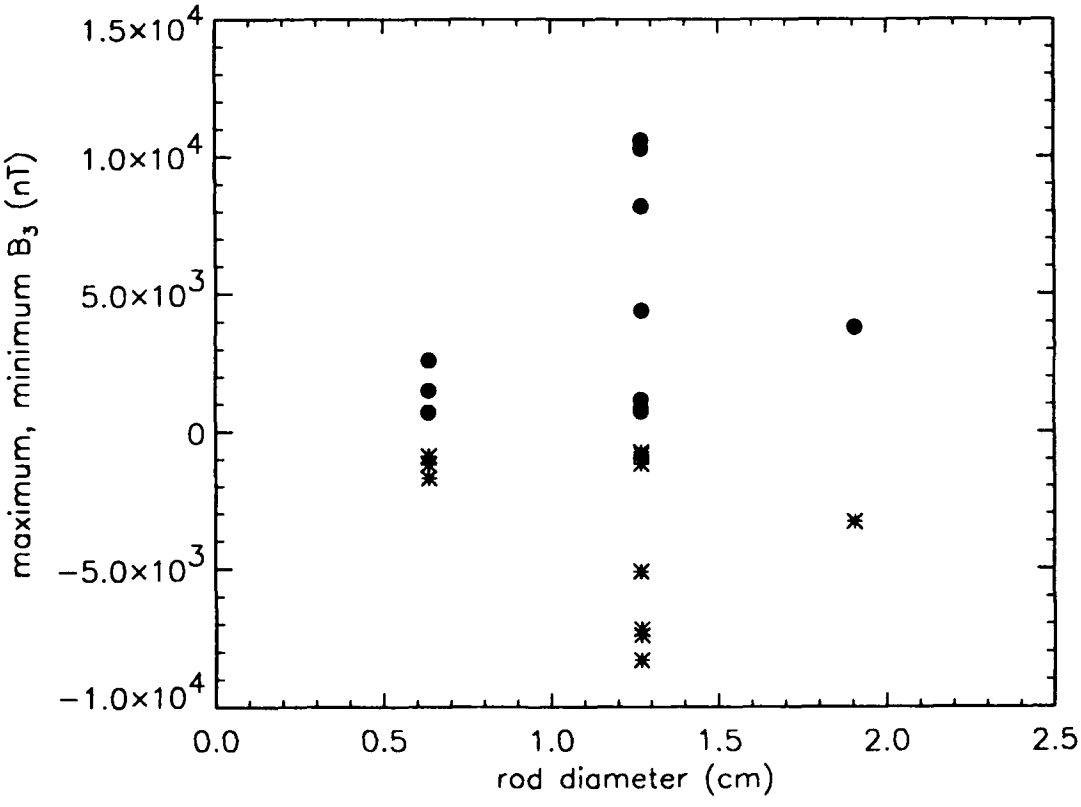

Figure 5.7

Maximum (dots) and minimum (stars) values of the magnetic field maps versus rod diameter for all rods at a depth of 13 cm.

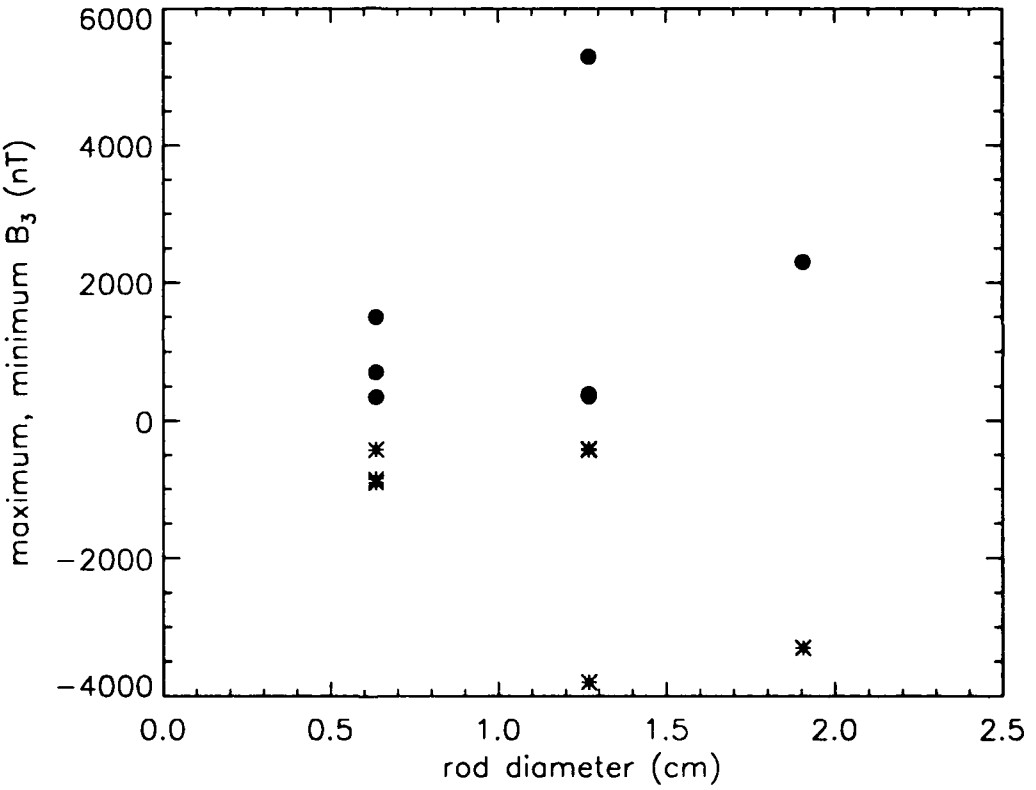

Figure 5.8

Maximum (dots) and minimum (stars) values of the magnetic field maps versus rod diameter for all rods at a depth of 18 cm.

6. Conclusions

A patented hand-held instrument has been built that is the first instrument to explicitly locate ferrous rods parallel to and buried behind or beneath a plane of measurement by analysing magnetic field and position data. The instrument has a number of useful applications, in particular the detection and characterization of reinforcing steel in concrete.

The instrument consists of a fluxgate magnetometer and position sensor unit enclosed in a small box which is moved by hand somewhat like a computer mouse. The sensor unit is connected by a cable to a processor unit, containing a microprocessor, A/D, displays and batteries. An operator scans the sensor unit over an area on the measurement surface, guided by the microprocessor, while the microprocessor controls the simultaneous collection of magnetic and position data. The microprocessor then uses simple algorithms to estimate the orientation, depth, length and diameter of the rod.

This report describes the final version of the instrument, originally designed to locate reinforcing rods in concrete. Experimental magnetic map data from horizontal rods are presented and compared to two simple models, the infinite cylinder and the long prolate spheroid. It was found that there was very poor agreement between both models and the experimental data.

Experiments using the instrument to estimate the parameters of a horizontal ferrous rod buried under a horizontal measurement plane are also described. It was seen that, for rod dimensions and geometry typical of reinforcing rods, all the location parameters, i.e., rod orientation in a horizontal plane, rod end locations (and hence rod length) and depth of rods could be estimated with reasonable accuracy at depths of 8 to 18 cm using very simple linear equations. Estimation of these parameters, however, required collection of position and magnetic data in two dimensions, since initially the rod orientation was unknown. Estimation of rod diameter was not possible with any degree of reliability chiefly due to the presence of substantial remnant magnetization.

Although this instrument represents a significant improvement in ferrous rod locator/identifiers, more research is necessary to develop a practical instrument.

The single biggest problem is the inability to determine rod diameter due to the presence of a large, variable remnant magnetization component in the rods. Future experiments should further investigate the nature of the remnant magnetization. It is desirable to know if the remnant magnetization is a function of the site, orientation or method of manufacture

of the rods. If this is so, one may be able to estimate the amount of remnant magnetization if some *a priori* information is available regarding the origin of the steel in the structure. In this regard, a suitable model is lacking. Numerical finite element magnetostatic modelling should be investigated to see if at least qualitative agreement between experimental and theoretical magnetic field values can be achieved.

If it is found that it is impossible to estimate remnant magnetization in advance, it may be possible to combine an active acoustic and magnetic sensor. The former would be used to estimate the diameter, while the latter would ensure that the detected object was definitely ferrous.

Other issues that should be addressed relate to instrument improvement. The location algorithms in the present instrument are very simple ones based on the infinite cylinder and not the ones that were found to best fit the experimental results. The instrument software must be modified to reflect this. At the same time, the obsolete MC6805 microprocessor should be replaced with a more modern processor such as the MC68HC11. This will allow more complicated processing of raw magnetic data to be performed, including perhaps the collection of complete magnetic maps, and allow a more user friendly interface, i.e., far less cryptic messages and menus. It will also greatly enhance code development and modification by allowing the use of high level programming languages. With its on-board A/D converter and EEPROM, it may be possible to put the entire microprocessor system in the sensor unit, thereby eliminating the separate processor unit and connecting cable. The motion noise of the existing instrument may be too high when operating on a rough concrete surface as opposed to a smooth table. One solution is to use a three-axis fluxgate sensor in place of a single-axis sensor. The former can be used to measure the total field and hence will have much smaller orientation sensitivity. The use of a two dimensional sensor unit ("mouse"), as originally envisioned, should be pursued. This would facilitate the collection of two dimensional position and magnetic data, which are required to estimate rod parameters, in an environment that is less controlled than that of the reported experiments.

Further tests also need to be done. The instrument should be tested on rods shallower than 8 cm and in the 18 to 30 cm depth range to ensure that algorithms are valid for the entire typical range of burial of reinforcing steel. Experiments should be conducted on horizontal rods at orientations other than north-south and on vertical rods, to determine whether the parameter estimation formulae are valid for different orientations. Experiments should also be conducted on nonisolated rods, such as would be found in typical situations where one encounters reinforcing steel.

7. References

[1] J.A.Bickley. Parking structure deterioration: a survey and analysis of its extent and influencing factors, vol 1 report. Technical Report T 4010-C, TROW Research, December 1984. Prepared for Canada Mortgage and Housing Corporation.

[2] J.E.McFee, Y.Das, and R.Ellingson. Locating and identifying compact ferrous objects. *IEEE Transactions on GeoScience and Remote Sensing*, GE-28(2):182–193, March 1990.

[3] J.E.McFee, R.Ellingson, and Y.Das. Experimental study of location and identification of ferrous spheroids using a smart total field magnetometer (U). Report SR-582, Defence Research Establishment Suffield, January 1993. UNCLASSIFIED.

[4] J.E.McFee, M.Bell, and G.Briosi. Mk 1 DREStector - an experimental prototype magnetometer for detection of structural steel in concrete (U). Memorandum SM-1129, Defence Research Establishment Suffield, August 1984. UNCLASSIFIED.

[5] J.R.Elliott and M.A.Woods. Rebar mouse (U). DRES Contractor Report Final Report, DSS Contract File No. W7702-6-2311-01-SG, Pylon Electronic Development Ltd., March 1987. UNCLASSIFIED.

[6] J.E.McFee. Magnetometer-based locator and identifier for ferrous objects having unknown shapes. United States Patent 102,379, June 6 1989.

[7] J.E.McFee. Ferrous object locator and classifier. Canadian Patent 1,267,192, March 27 1990.

[8] J.E.McFee. Electromagnetic remote sensing - low frequency electromagnetics (U). Special Report SSP-124, Defence Research Establishment Suffield, January 1989. UNCLASSIFIED.

[9] W.Smythe. *Static and dynamic electricity third edition.* McGraw-Hill, New York, 1968.

[10] J.E.McFee, M.Bell, B.Dempsey, R.Chesney, and Y.Das. A magnetostatic signature measurement and analysis system. *Journal of Physics E*, 18:54–60, January 1985.

[11] J.E.McFee and Y.Das. A multipole expansion model for compact ferrous object detection. In *Proceedings of the ANTEM Symposium on Antenna Technology and Applied Electromagnetics*, pages 633–638, University of Manitoba, Winnipeg, MN, Canada, August 1990.

[12] J.F.Scarzello, R.H.Lundsten, C.W.Purves, A.M.Syeles, and W.R.Grine. Development of a Brown magnetometer with solenoidal sense windings (U). Technical Report NWSC TR 82-96, Naval Surface Weapons Center, 1981. UNCLASSIFIED.

[13] R.E.Brown. A pulse-driven fluxgate magnetometer requiring very low power (U). Technical Report NWSC TR 80-161, Naval Surface Weapons Center, 1980. UNCLASSIFIED.

[14] J.Simkin and C.Trowbridge. Three-dimensional nonlinear electromagnetic field computations using scalar potentials. *IEE Proceedings*, 127B:368–374, 1980.

[15] P.R.Bevington. *Data reduction and error analysis for the physical sciences*. McGraw-Hill, New York, 1969.

DOCUMENT CONTROL DATA

(Security classification of title, body of abstract and indexing annotation must be entered when the overall document is classified)

1. ORIGINATOR (the name and address of the organization preparing the document. Organizations for whom the document was prepared, e.g. Establishment sponsoring a contractor's report, or tasking agency, are entered in section 8.)

Defence Research Establishment Suffield
Box 4000, Medicine Hat, Alberta T1A 8K6

2. SECURITY CLASSIFICATION (overall security classification of the document including special warning terms if applicable)

Unclassified

3. TITLE (the complete document title as indicated on the title page. Its classification should be indicated by the appropriate abbreviation (S,C,R or U) in parentheses after the title.)

Estimation of Depth, Orientation, Length and Diameter of Long Horizontal Ferrous Rods using a Fluxgate Magnetometer (U)

4. AUTHORS (Last name, first name, middle initial. If military, show rank, e.g. Doe, Maj. John E.)

McFee, John; Ellingson, Robert; Elliott, John and Das, Yodadhish

5. DATE OF PUBLICATION (month and year of publication of document)

April 1993

6a. NO. OF PAGES (total containing information. Include Annexes, Appendices, etc.)

84

6b. NO. OF REFS (total cited in document)

15

6. DESCRIPTIVE NOTES (the category of the document, e.g. technical report, technical note or memorandum. If appropriate, enter the type of report, e.g. interim, progress, summary, annual or final. Give the inclusive dates when a specific reporting period is covered.)

Suffield Report 585

8. SPONSORING ACTIVITY (the name of the department project office or laboratory sponsoring the research and development. Include the address.)

Chief Research and Development,
Director Military Engineering (D Mil E)

9a. PROJECT OR GRANT NO. (if appropriate, the applicable research and development project or grant number under which the document was written. Please specify whether project or grant)

031SD and 27B77 (Task DMER 15)

9b. CONTRACT NO. (if appropriate, the applicable number under which the document was written)

10a. ORIGINATOR'S DOCUMENT NUMBER (the official document number by which the document is identified by the originating activity. This number must be unique to this document.)

SR 585

10b. OTHER DOCUMENT NOS. (Any other numbers which may be assigned this document either by the originator or by the sponsor)

11. DOCUMENT AVAILABILITY (any limitations on further dissemination of the document, other than those imposed by security classification)

(X) Unlimited distribution
( ) Distribution limited to defence departments and defence contractors; further distribution only as approved
( ) Distribution limited to defence departments and Canadian defence contractors; further distribution only as approved
( ) Distribution limited to government departments and agencies; further distribution only as approved
( ) Distribution limited to defence departments; further distribution only as approved
( ) Other (please specify):

12. DOCUMENT ANNOUNCEMENT (any limitation to the bibliographic announcement of this document. This will normally correspond to the Document Availability (11). However, where further distribution (beyond the audience specified in 11) is possible, a wider announcement audience may be selected.)

13. **ABSTRACT** (a brief and factual summary of the document. It may also appear elsewhere in the body of the document itself. It is highly desirable that the abstract of classified documents be unclassified. Each paragraph of the abstract shall begin with an indication of the security classification of the information in the paragraph (unless the document itself is unclassified) represented as (S), (C), (R), or (U). It is not necessary to include here abstracts in both offical languages unless the text is bilingual).

A patented hand-held instrument has been built that is the first instrument to explicitly locate ferrous rods parallel to and buried behind or beneath a plane of measurement by analysing magnetic field position data. The instrument has several useful applications, in particular the detection and characterization of reinforcing steel in concrete.

The instrument consists of a fluxgate magnetometer and position sensor unit enclosed in a small box which is moved by hand somewhat like a computer mouse. A cable connects the sensor unit to a processor unit, containing a microprocessor, A/D, displays and batteries. An operator scans the sensor unit over the measurement surface, guided by the microprocessor, which controls the simultaneous collection of magnetic and position data. The microprocessor then uses simple algorithms to estimate location parameters, rod length and diameter.

This report describes the final version of the instrument. Experimental magnetic data from horizontal rods are presented and compared to two simple models, the infinite cylinder and the long prolate spheroid. It was found that there was very poor agreement between both models and the experimental data.

Experiments using the instrument to estimate the parameters of a horizontal ferrous rod buried under a horizontal measurement plane are also described. It was seen that all the location parameters (rod orientation, end locations, depth) of typical reinforcing rod could be estimated with reasonable accuracy at depths of 8 to 18 cm using very simple linear equations. Estimation of rod diameter was unreliable chiefly due to the presence of substantial remnant magnetization.

14. **KEYWORDS, DESCRIPTORS or IDENTIFIERS** (technically meaningful terms or short phrases that characterize a document and could be helpful in cataloguing the document. They should be selected so that no security classification is required. Identifiers, such as equipment model designation, trade name, military project code name, geographic location may also be included. If possible keywords should be selected from a published thesaurus. e.g. Thesaurus of Engineering and Scientific Terms (TEST) and that thesaurus-identified. If it is not possible to select indexing terms which are Unclassified, the classification of each should be indicated as with the title.)

REINFORCING STEEL
REINFORCING ROD
CONCRETE
REBAR
MAGNETOMETER
FLUXGATE
MAGNETIC FIELD
POSITION
DETECT
LOCATE
IDENTIFY
MODEL
SPHEROID
CYLINDER
MICROPROCESSOR
REMNANT